CHARGE SPECTRUM OF THE HEAVY PRIMARY COSMIC RAYS

Thesis by

Edward Abraham Stern

In Partial Fulfillment of the Requirements

for the Degree of

Doctor of Philosophy

California Institute of Technology

Pasadena, California

1955

ACKNOWLEDGMENTS

In the design of new equipment one always meets with various difficulties. The research described in this thesis was performed under the supervision of Dr. H. V. Neher whose contribution of some very important ideas was essential in the overcoming of these obstacles. The author is also indebted to Dr. Neher for his constant interest in the research and for many very stimulating discussions.

It is also a pleasure to acknowledge the help of Mr. Alan Johnston whose aid was essential in collecting the data during the balloon flight. In addition Mr. Johnston read over a section of the preliminary thesis and made some suggestions that were greatly appreciated.

Although only two sets of equipment were successfully flown, twelve sets were constructed in all. Such a formidable construction job would have been extremely tedious without the aid of various undergraduates, most of whom were at the time members of the author's freshman physics class. The help of Earl Jacobs is also gratefully acknowledged. His inspiration and help came at a critical moment when time was short and the work was long.

The skyhook balloon flight was sponsored by the Office of Naval Research as was the rest of the research. The cooperation of the ONR representative, Commander Sparkman, who arranged the skyhook balloon flight, is gratefully acknowledged.

Finally it is with pleasure that I thank the National Science Foundation for two fellowships which covered the time of the research of this thesis.

ABSTRACT

A measurement at $\lambda = 55^{\circ}$ and 95,000 feet was made of the heavy primary cosmic-ray charge spectrum ($Z > 3$) by means of a pulse ionization chamber. The characteristics of the chamber and associated electronics are described.

The effect of nuclear stars on the counting rate of the chamber was determined experimentally by sending up simultaneously two chambers, one filled with argon at half the pressure of the other. Slow evaporation particles will stop in the chambers and give the same pulses independent of pressure. Cosmic rays give pulses proportional to the gas pressure. Comparing the two chamber counting rates permits a determination of the star contribution.

Other causes of the background counting rate were discussed and corrected for. It was concluded that Be and B combined are as abundant in the primary beam as the CNO group. The flux of the heavy particles $Z \geq 9$ was also determined. It was not possible to obtain any information on the abundance of Li.

A suggested improved version of the equipment is described and possible experiments are discussed.

TABLE OF CONTENTS

INTRODUCTION

To date practically all of the quantitative data on the heavy flux $Z \geq 3$ have been obtained by means of photographic emulsions. At the time that this experiment was conceived photographic emulsion data disagreed on the existence of Li, Be, and B in the primary beam [19,20], though they did agree on the intensity of the CNO group and the $Z > 9$ group. Since then the data have agreed on the existence of Li, Be, and B [18] but disagreed on their intensity. However, even in the CNO group there was disagreement among photographic people on the relative intensities of C, N, and O within the group. [19,20] In addition there was disagreement on the energy spectrum of the heavy particles measured in the emulsion. [19,20] For these reasons and others it seemed desirable to obtain measurements on the heavy flux by an independent means, in this case the pulse ionization chamber.

Pulse ionization chambers had been used before to measure the primary flux $Z \geq 3$ but only to show that the pulse size distribution was consistent with the spectrum obtained by photographic plates. Pulse ionization chambers have also been used to measure the primary α-particle flux and have given some semi-quantitative results. [23]

The importance of the determination of the heavy cosmic-

ray flux for theories on the origin of cosmic rays has been amply discussed in the literature [19,20,21] and will not be attempted here.

A decided disadvantage of photographic plates is the great amount of work necessary to obtain any statistics on ionizing events and, in particular, the heavy particle flux. Electronic devices can accumulate the statistics much more readily and are thus better suited for measurements of time fluctuations of the intensity of the heavy particles.

It has recently been realized that [24] studies of fluctuations in the intensity of cosmic rays will throw some light on the origin of cosmic rays and on the structure of the solar system. This makes it increasingly important to develop electronic equipment to measure reliably the heavy particle flux.

DESCRIPTION OF THE EQUIPMENT

THE PULSE IONIZATION CHAMBER

The instrument used in this experiment is a pulse ionization chamber which employs electron collection. Electrons formed by an ionizing particle traversing the chamber are collected on the collecting electrode consisting of a 2" diameter hollow copper sphere supported by a .110" diameter copper plated drill rod in the center of a 10" diameter thin walled steel spherical shell. The voltage pulse induced on the center electrode by the collected electrons is amplified, and both the number and sizes of the voltage pulses are telemetered to ground. The chamber is operated with 300 volts between the collecting electrode and the outer shell, and is filled with either about 3 or $1\frac{1}{2}$ atmospheres pressure of 99.9986 percent pure argon. The instrument is calibrated both before and during a flight by means of a Po^{210} α-particle source built permanently inside the chamber. The voltage across the chamber is sufficient to saturate the pulses due to the Po α-particles.

The Po^{210} was placed on a clean copper electrode by merely rubbing the electrode on some Po^{210} plated copper foil. The adhesion was strong enough to coat the electrode with a sufficient amount of Po^{210}. The Po electrode was insulated from

the rest of the chamber by being soldered in a kovar seal, which was itself soldered to the sphere. The construction details are shown in Figure 1. By changing the voltage on the Po electrode similar to the way it was done by Pomerantz [1], it is possible to turn the Po α-particle pulses on and off. When the Po electrode was connected to the spherical shell at +300 volts the electrons from the ions formed by the α's were collected by the center electrode, turning the pulses on. When the Po-α electrode was grounded, thus being at the same voltage as the center electrode, the electrons were collected on the Po electrode and did not reach the center electrode, turning the α pulses off. During the flight a clock driven switch turned the α pulses on and off periodically to give a standard pulse as a check on the stability and accuracy of both the receiving and the balloon equipment.

Design Details

The size of the center electrode was determined by various requirements. In designing equipment for balloon flights it is desirable to have everything as light and simple as possible without undue sacrifice in quality of performance. The voltage which must be maintained across the ionization chamber should be as low as possible, but still must be able to collect the electrons from an ionizing particle. Less voltage means smaller number of batteries

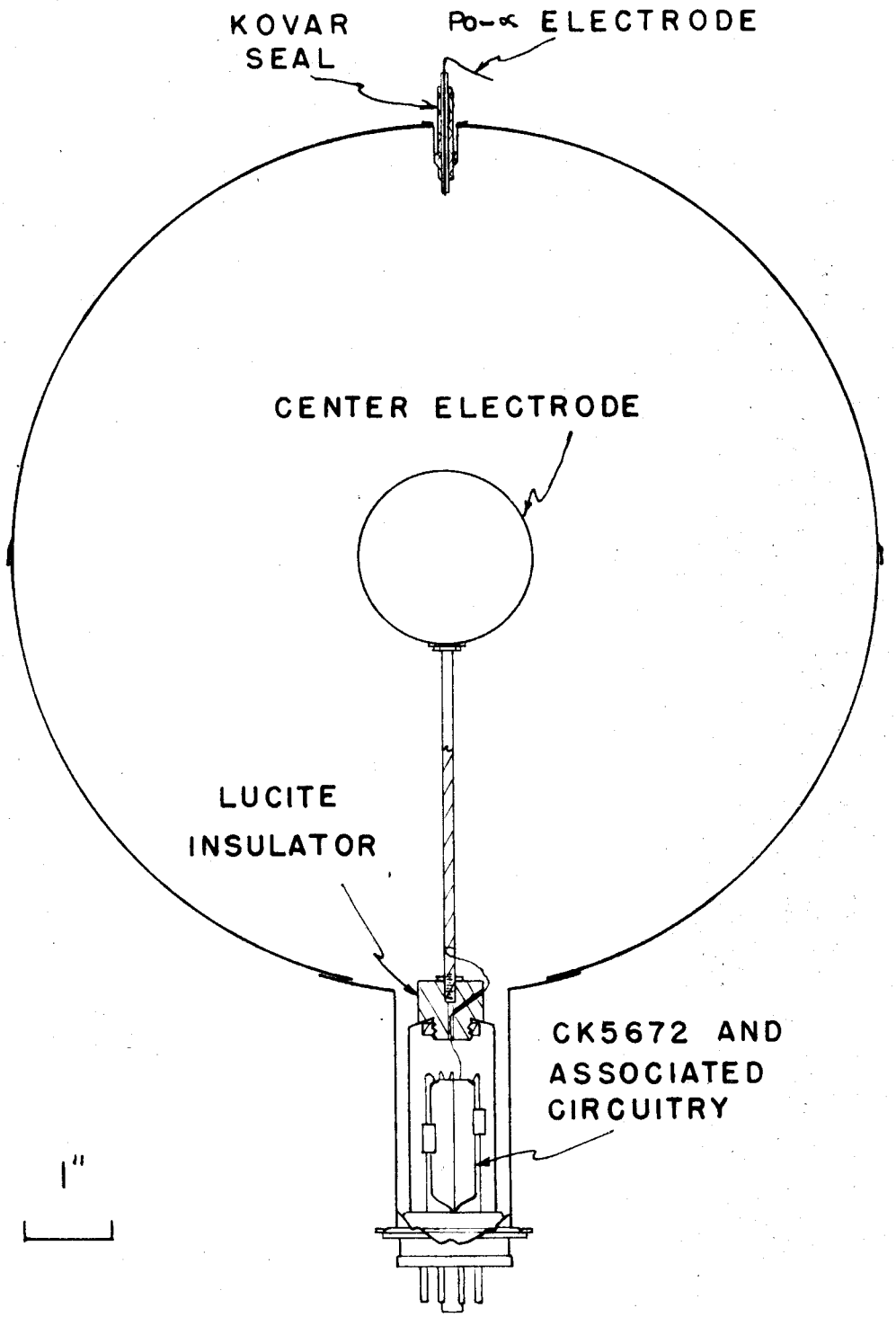

Figure 1. Construction details of the pulse ionization chambers.

required and, hence, less weight. In addition by using low voltages across the chamber the dangers of spurious pulses due to sparking and corona at high altitudes will be lessened. The quantity of importance in collecting electrons for a given pressure is the electric field and, in particular, the electric field next to the outer sphere where it is weakest. Increasing the size of the center electrode will, for a given potential across the sphere, increase the electric field.

There is another effect dependent on the size of the center electrode that is very important. In electron collection, where the electrons are collected much more rapidly than the positive ions and where the decay time constant of the amplifier is adjusted so that the amplifier amplifies only the fast pulse induced by the electron collection, the amount of charge induced on the center electrode by a collected electron depends on where the ion pair from which the electron came is formed in the chamber.[2] If the potential of the center electrode is called 0 and that of the outer electrode V_o, then the amount of charge induced on the center electrode when an electron is collected, is, $e\frac{V}{V_o}$, where V is the potential where the ion pair was formed and e the electronic charge.[2]

This effect, the potential factor, can be readily calculated for spherical geometry. It is sufficient to calculate the differential pulse height distribution produced in the chamber by a unidirectional beam of similar particles

which lose an average energy per unit path length in the chamber of w. Fluctuation in energy loss will be neglected now but will be considered later. The assumption will be made, borne out experimentally [3], and also expected theoretically [4], that the average number of ion pairs formed is proportional only to the energy loss of a particle and not dependent on the energy or type of particle. Under the assumed conditions the pulse height will vary because of varying path lengths through the chamber and because of the potential factor.

Consider a particle which traverses a length ℓ through a chamber of radius b (see Figure 2). Call $R = \sqrt{b^2 - (\frac{\ell}{2})^2}$ the shortest distance between the path of the particle and the center of the sphere. The number of ion pairs formed in a length dx is $\frac{w}{W_o}$ dx where W_o is the average energy per nucleon pair. It will be assumed that all ion pairs are formed near dx. This is not precisely true since high energy knock-on electrons from a relativistic particle will travel appreciable distances, ionizing along their paths, before they will stop. However the greatest portion of the energy loss for relativistic cosmic-ray particles is by low energy collisions producing low energy electrons which produce all of their ionization near their point of formation. The high energy knock-ons will be emitted preferentially in the direction of the incident particle and will form most of their ions in the vicinity of the original path of the

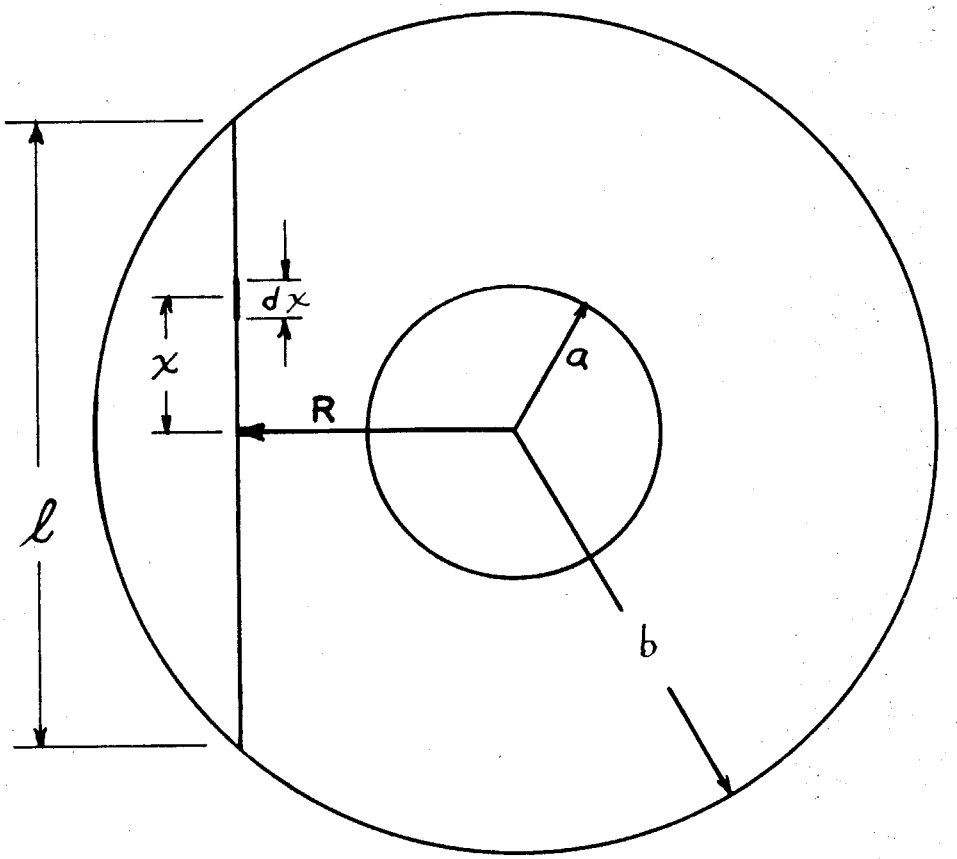

Figure 2. Diagram explaining the meaning of the symbols involved in calculating the potential factor for a spherical chamber.

primary particle. For these reasons the assumption is valid.

The voltage induced on the center electrode by the ion pairs formed in dx is

$$dS(\ell) = \frac{ewV}{W_o V_o} \, dx .$$

$$\frac{V}{V_o} = \frac{\frac{1}{r} - \frac{1}{a}}{\frac{1}{b} - \frac{1}{a}} = \frac{b(a-r)}{r(a-b)} ,$$

where r is the distance of the element dx from the center of the sphere. The total voltage induced on the center electrode is

$$S(\ell) = \frac{ewb}{W_o(a-b)} \int \frac{(a-r)\, dx}{r} .$$

Consider case (a) where $R \geq a$, the particle does not pass through the center electrode.

$$R^2 + x^2 = r^2,$$

where x is shown in Figure 2.

$$dx = dr \, \frac{r}{x} = \frac{r \, dr}{\sqrt{r^2 - R^2}} .$$

$$S(\ell) = \frac{2ewb}{W_o(a-b)} \int_R^b \frac{(a-r)}{\sqrt{r^2-R^2}}\, dr$$

$$= \frac{2ewb}{W_o(a-b)} \left[a \ln\left(\frac{b + \ell/2}{b^2 - (\ell/2)^2} \right) - \frac{\ell}{2} \right],$$

$$0 \leq \ell \leq 2\sqrt{b^2-a^2}\ .$$

Define

$$Q(\ell) \quad \frac{S(\ell)\ W_o\ (a-b)}{2ewb}\ . \qquad (1)$$

Then

$$Q(\ell) = a \ln\left(\frac{b+\ell/2}{\sqrt{b^2-(\ell/2)^2}} \right) - \ell/2\ , \qquad 0 \leq \ell \leq 2\sqrt{b^2-a^2},$$

$$= a \ln\left(\frac{b+\sqrt{b^2-R^2}}{R} \right) - \sqrt{b^2-R^2}\ , \qquad b \geq R \geq a. \quad (2)$$

Consider now case (b) where $R \leq a$, the particle passes through the center electrode.

$$Q(\ell) = \int_a^b \frac{a-r}{\sqrt{r^2-R^2}}\, dr = a \ln\left(\frac{b+\ell/2}{a+\sqrt{a^2-R^2}} \right) - \frac{\ell}{2} + \sqrt{a^2-R^2}\ ;$$

$$0 \leq R \leq a\ . \qquad (3)$$

The probability of a particle passing in the interval $R \rightarrow R + dR$ is

$$P(R)\, dR = \frac{2\pi R}{K}\, dR,$$

where K is a normalizing constant determined so that

$$\int_o^b P(R)\, dR = 1 = \frac{\pi}{K}\int_o^b 2R\, dR = \frac{\pi b^2}{K} . \qquad K = \frac{1}{b^2} ,$$

and

$$P(R)\, dR = \frac{2R\, dR}{b^2} \tag{4}$$

We next introduce $q(Q)$ as the probability that the pulse height is between Q and Q + dQ.

Then $q(Q)\, dQ = P(R)\, dR$,

$$\text{or } q(Q) = P(R)\frac{dR}{dQ} = \frac{2R}{b^2}\ \frac{dR}{dQ} = \frac{2R}{b^2}\ \frac{1}{\frac{dQ}{dR}} \tag{5}$$

To determine $\frac{dQ}{dR}$ we differentiate Equations 1 and 2, and after much mental exercise in algebra, we obtain

$$\frac{dQ}{dR} = \frac{R^2 - ab}{R\sqrt{b^2 - R^2}} , \qquad b \geq R \geq a , \tag{6a}$$

$$\frac{dQ}{dR} = \frac{R}{\sqrt{b^2-R^2}}\left[1 - \frac{a}{b+\sqrt{b^2-R^2}} - \frac{b}{a+\sqrt{a^2-R^2}}\right.$$

$$\left. + \frac{R^2}{(b+\sqrt{b^2-R^2})(a+\sqrt{a^2-R^2})}\right], \qquad a \geq R \geq 0 \qquad (6b)$$

Combining Equations 5 and 6 we obtain our desired differential pulse height distribution. It is of interest to note that the relation between Q and R is double valued; at some values of Q there exist two values of R. In order to find q(Q) for these values of Q one has to add

$$P(R_1)\left(\frac{dR}{dQ}\right)_{R_1} \quad \text{and} \quad P(R_2)\left(\frac{dR}{dQ}\right)_{R_2},$$

where R_1 and R_2 are the two values corresponding to Q. The distribution q(Q) was calculated graphically and is given in Figure 3 for a 2" diameter center electrode and 10" diameter outside electrode. For comparison the differential distribution for a zero diameter center electrode is plotted. It is seen that the differential pulse height distribution is greatly improved towards an ideal one by using a 2" diameter center electrode. The integral pulse height distributions

$\int_{Q}^{Q_{max}} q(Q')\,dQ'$ are given in Figure 4 for a 2" diameter

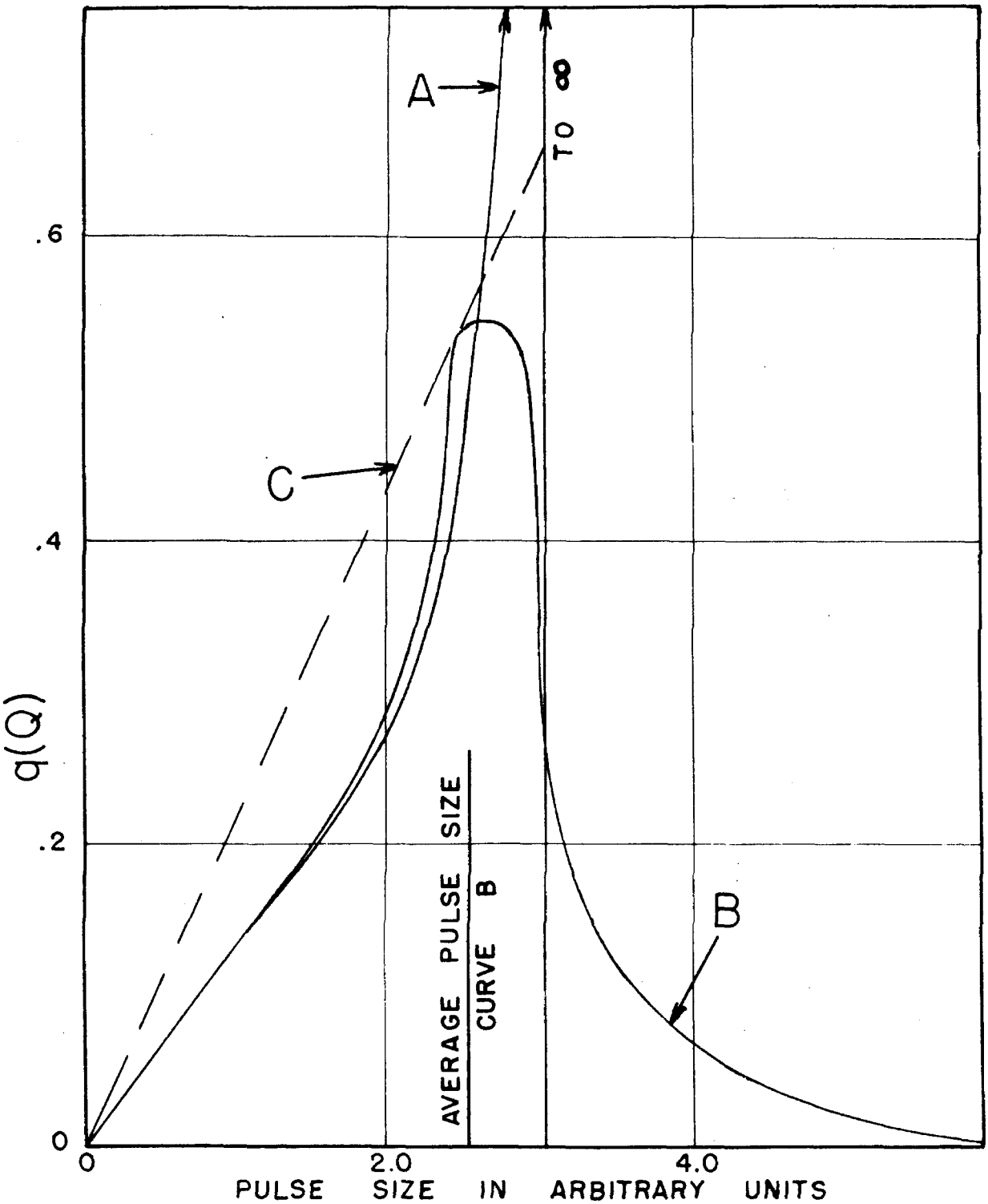

Figure 3. The differential pulse height distribution $q(Q)$ caused by similar particles passing through a spherical pulse ionization chamber. Curve A is for a 2" diameter center electrode and a 10" diameter outside electrode with no statistical fluctuations. Curve B is for the same dimensions as Curve A but the statistical fluctuations in energy loss are included when the pressure of argon in the chambers is a few atmospheres. Curve C is for a 0" center electrode and a 10" diameter outside electrode with no statistical fluctuations.

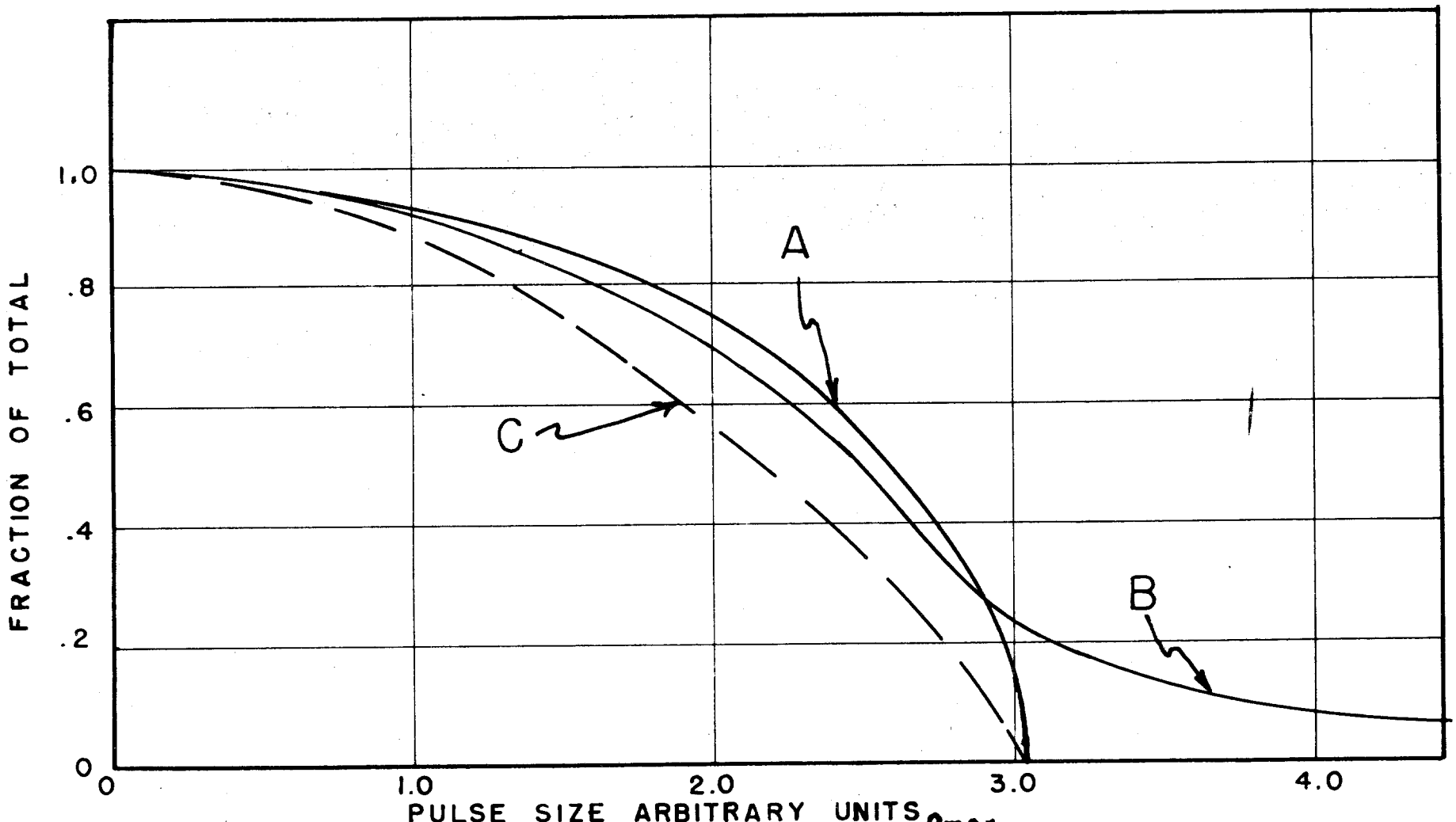

Figure 4. The integral pulse height distribution, $\int_{Q}^{Q_{max}} q(Q)\,dQ$, caused by similar particles passing through a spherical pulse ionization chamber. Curves A, B, and C are the integral distributions of Curves A, B, and C in Figure 3, respectively.

and a 0" diameter center electrode.

The maximum pulse occurs when $\frac{dQ}{dR} = 0$ or from Equation 6a when $R = \sqrt{ab}$. Using this and Equations 1 and 2 we see that the ratio of the maximum pulse for a = 1" and a = 0 with b = 5" is

$$\frac{S_{max,\ a=1}}{S_{max,\ a=0}} = .757 \quad . \tag{7}$$

One may ask what is the value for a, the center electrode radius, that will give the best differential pulse height distribution. A larger a than 1" would improve the pulse height distribution but would introduce other practical difficulties. The larger the center electrode is, the harder it is to support it. The larger the center electrode, the more are the nuclear stars that are formed in it. It is desirable to minimize the number of nuclear stars since they can give pulses that can be confused with cosmic-ray primaries. More will be said about nuclear stars later. In addition it will be shown that if the statistical fluctuations in ionization are taken into account they cause a spread in pulse sizes that is surprisingly large, preventing much gain by increasing a.

The gas pressure used in the chamber is determined by considerations of recombination, the effect of nuclear stars, and the desired pulse sizes. For a given chamber the number

of ion pairs formed by a particle traversing a region of the chamber is proportional to the gas pressure. Assuming all of the electrons formed are collected the pulse height will be proportional to the pressure. Increasing the pressure decreases the required gain of the amplifier, which is desirable because this means less batteries, weight, and tubes are needed. On the other side, increasing the gas pressure requires greater voltages across the sphere to collect all of the electrons formed.

The pulse height due to Po α-particles vs. voltage is plotted in Figure 5 for 60 p.s.i. sphere pressure and a 1" diameter center electrode (These are not the same operating conditions used in the flight). It is seen that the Po-α pulse height is not completely saturated till about 600-700 volts. Below 600 volts not all of the electrons are collected. Above 700 volts it is assumed that all of the electrons are collected. Other observers [2,5] have presented good evidence to show that saturation means that essentially all electrons are collected. For the design that was finally decided upon (2" diameter center electrode, 10" diameter outer electrode, 3 atmospheres of argon, and 300 volts across the chamber), the Po-α pulses were saturated. Increasing the voltage to 600 volts changes the Po-α pulse height by less than 5 percent. As a check that no appreciable recombination or attachment of electrons was occurring under the operating conditions, the maximum pulse height due to Po-α's

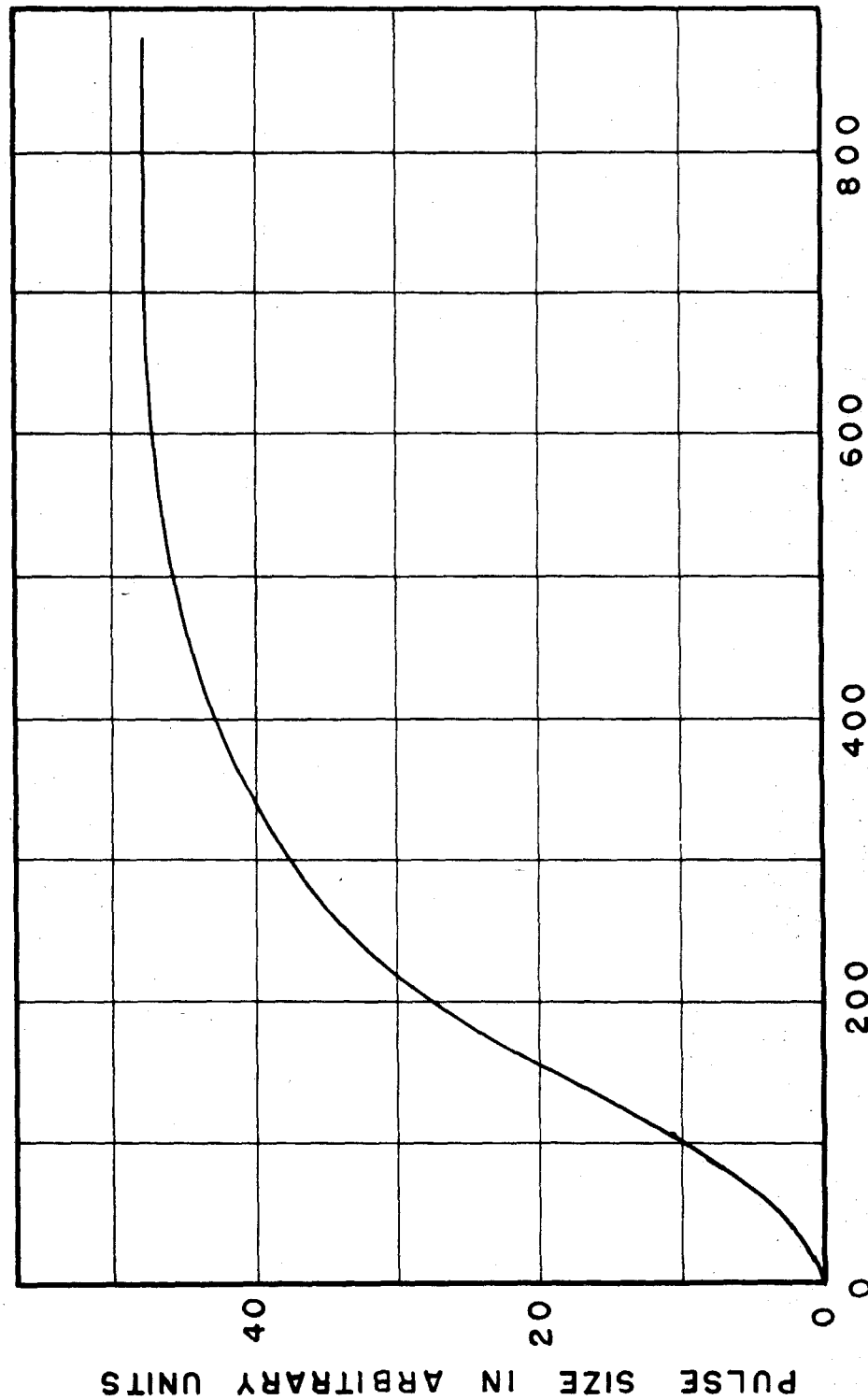

Figure 5. The maximum pulse height of Po^{210} α-particles as a function of the voltage across a 10" diameter outer electrode and a 1" diameter inner electrode pulse ion chamber filled with 60 psi of argon. It is seen that the pulse size reaches saturation after 700 volts. These are not the operating conditions of the chambers used in this experiment.

was measured at 5 p.s.i. absolute with 50 volts across the chamber and 300 volts across the chamber. The maximum pulse height did not change more than 3 percent from the maximum pulse height under operating conditions. The maximum pulse height was determined by running an integral pulse height measurement. To run this test the same electronics as used during a flight was employed (see next section on electronics). The output from the amplifier went to the biased tube, which grid was disconnected from the sawtooth bias generator and connected to a variable potential supply. The output from the one-shot multivibrator was connected to a scalar and measurements taken. A typical integral pulse height curve is given in Figure 6.

The number of nuclear stars produced in the gas of the ionization chamber is proportional to the mass of the gas, which for a given volume and temperature is proportional to the pressure. The pulses due to nuclear star evaporation particles are approximately independent of the pressure for the pressures used in the chambers because they stop in the chamber. The pulses due to cosmic-ray particles which pass through the chamber are proportional to the pressure. The integral pulse height counting rate at a given pulse height, will increase with increasing gas pressure partly because the number of stars has increased, and also because this pulse size will now correspond to smaller charged cosmic-ray particles, which are, as a rule, more numerous. The best

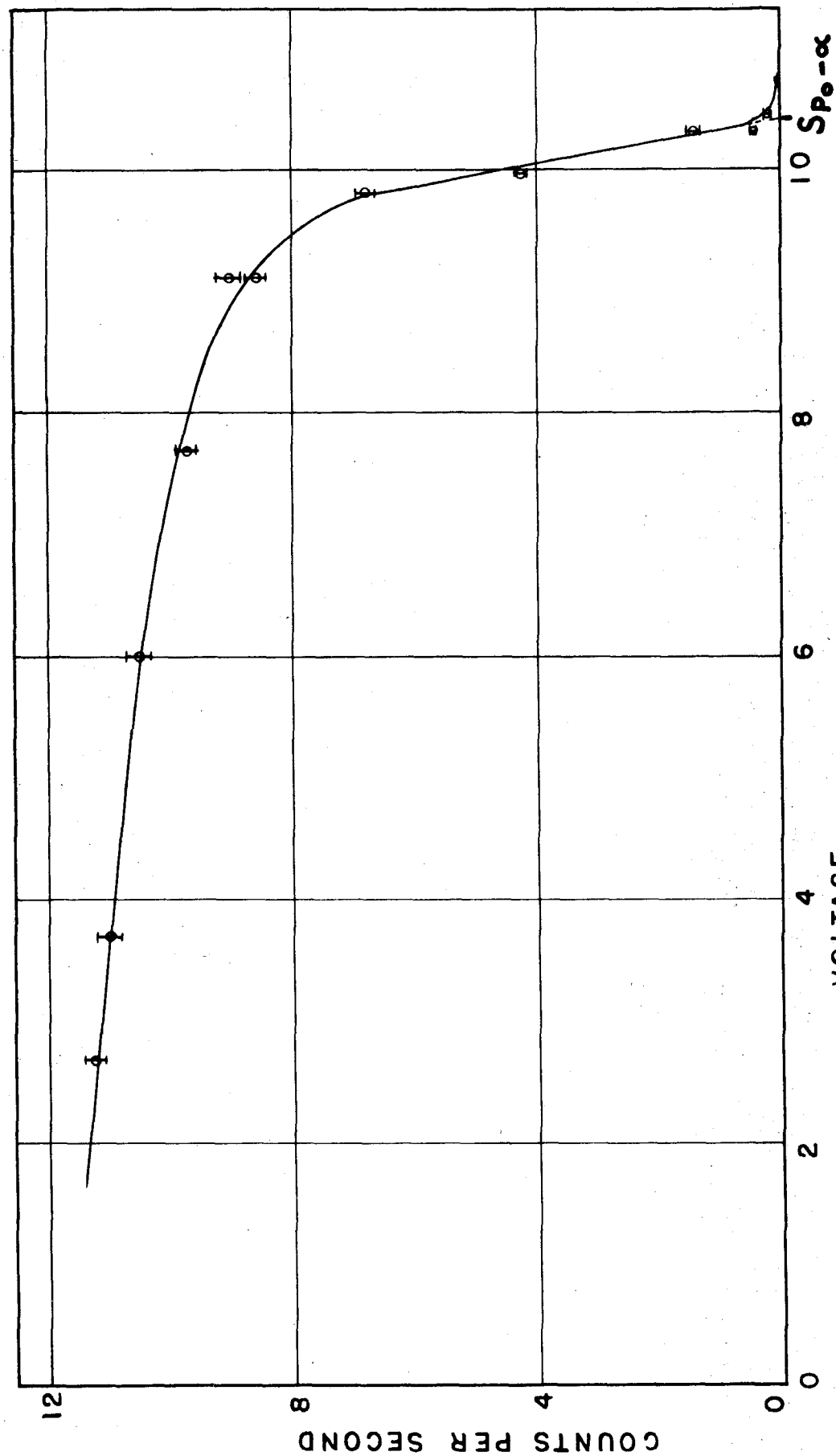

Figure 6. Integral pulse height curve for Po^{210} α-particles. The maximum pulse is indicated as an extrapolation of the steep slope of the curve.

situation exists when the counts due to nuclear stars are the smallest fraction of cosmic-ray counts. For the pressures used in the present experiment it happened to be true that most of the stars detected were formed in the chamber wall (see discussion under nuclear stars) so that the number of nuclear stars did not increase in proportion to the pressure, but more slowly. However at high pressures, where the wall effect is negligible, the effect of nuclear stars should be proportional to the pressure. The optimum pressure to minimize the relative effect of nuclear stars depends on what Z particles one is trying to measure. By looking at the integral pulse height curve obtained in this experiment due to cosmic-ray particles (see Figure 14) one can determine the approximate effect on the counting rate of changing the pressure. If increasing the pressure by a certain factor will increase the counting rate by a greater factor, then, as far as minimizing the effect of stars is concerned, one can gain by increasing the pressure. By this means it is seen from Table IV and Figure 14 that, for the size chamber used, the pressure of 3 atmospheres is about optimum for measuring Li, Be, B, C, N, and O nuclei, but higher pressures would improve the situation for the higher Z particles.

Higher gas pressures are advantageous in another respect. The effect of statistical fluctuations has been calculated by Landau [6] and Symon.[7] The effect of these fluctuations

will be to spread out the differential pulse height distribution of the chamber, and it is thus desirable to minimize these fluctuations. Greater gas pressure will cause a particle to lose more energy in passing through the chamber reducing the percentage fluctuation. However, surprisingly, this reduction for amounts of matter of a gram or so is very little. For example, the percentage spread [$\frac{\Delta_c}{E_o - E_p}$ in Reference 7] for a 2 Bev singly charged proton passing through .118 g/cm^2 of argon is 10.1 percent. For the same particle passing through 4 times as much argon the same measure of the percentage spread is still 9.2 percent. Unless one goes to very much higher pressures there will not be much gain.

It is important to calculate these statistical fluctuations because they affect significantly the differential and integral pulse distributions of the chambers. The calculations of Landau and Symon are for Z = 1 particles. Their results can be immediately used for higher Z particles by using for particles of charge Z passing through an amount of matter x the results calculated for a singly charged particle passing through Z^2x amount of matter. This can be proved by using the results of Landau. He shows by means of the LaPlace transform [8] that

$$f(x,\Delta) = \frac{1}{2\pi i}\int_{-i\infty+\sigma}^{+i\infty+\sigma} e^{+P\Delta - x\int w(\varepsilon)(1-e^{-P\varepsilon})\,d\varepsilon}\,dP$$

where $f(x,\Delta)$ is the probability that a particle of a given initial energy E_o on traversing an amount of matter x will lose an amount of energy between Δ and $\Delta + d\Delta$, $w(\varepsilon)$ is the probability per unit length of path of an energy loss ε. $w(\varepsilon)$ is proportional to Z^2 and we see that Z^2 and x enter into $f(x,\Delta)$ only in the combination Z^2x, which justifies the procedure.

This calculation was performed numerically for Chamber No. 14, in which the density of argon is 5.20 g/liter. The results for the differential pulse height distribution are shown in Figure 3, and those for the integral pulse height distribution in Figure 4. The energy loss of 1.49 Mev/g - cm^{-2} in argon for a singly charged minimum ionizing particle was used in the calculation. Although Chamber No. 13 had half the pressure of Chamber No. 14, this makes only a negligible change in its pulse height distribution.

At first sight it may seem that not all of the energy lost by a particle will be measured by the chambers because high energy delta rays produced in the chambers will escape before losing all of their energies. This would have the effect of making the high energy tail of the differential distribution function of energy loss fall off more sharply than the calculations indicate. These high energy delta rays have of the order of 200 kev and greater energies. For these high energy collisions the probability of a collision is independent of the structure of the atom but depends only

on the density of electrons, i.e., the energy loss per g - cm^{-2} taken away by these high energy delta rays depends only on Z/A of the material, where Z is the number of electrons in an atom and A is the atomic weight of the material. Argon, air, and steel have about the same Z/A.

If we assume that delta rays with energies greater than 200 kev are ejected essentially along the path of the primary particle, which should be mostly true in these high energy collisions, then the energy loss measured in the chamber should be the <u>total</u> energy loss. For every high energy delta ray that escapes from the chamber there will be, on the average, another corresponding high energy delta ray that was produced above the sensitive part of the chamber, in the wall or the air above, and will enter the chamber, ionizing and replacing the energy lost when the delta ray produced in the gas escaped.

This can be seen by considering a particle which ionizes along a long path, x g/cm^2, but the average energy loss per g - cm^{-2}, k, along the path remains constant. The total energy loss is then kx and the energy loss measured along a small portion of the path dx is on the average just $kx \frac{dx}{x} = k\ dx$.

The actual fluctuations in the pulse height will be greater than the fluctuations in energy loss alone, because, in addition to these fluctuations, the pulse height will be affected by fluctuations in the number of ion pairs formed

for a given energy and by fluctuations in the density of ionization along the path, which affect the pulse height because of the potential factor. Since there is no theory to calculate the effect of the other fluctuations, the true fluctuation in pulse height will be assumed to be that of the statistical fluctuations in energy loss of particles passing through the chamber. Experimentally there is evidence that the actual fluctuations in pulse height are only slightly greater than that calculated from energy losses alone.[9]

ELECTRONICS

A block diagram of the electronics that accompanies the ionization chamber on its balloon flight is shown in Figure 7a. The pulses induced on the collecting electrode of the ionization chamber are amplified by the amplifier. The output pulses are fed into the biased tube whose bias voltage is continuously varying. Only pulses larger than a value determined by the bias voltage at any time can pass through the biased tube and trigger the one-shot multivibrator. The multivibrator feeds a positive square pulse onto the grid of the transmitting tube which is otherwise biased off, and starts it transmitting for about a millisecond.

The amplifier used 3 tubes connected to operate as a negative feedback linear amplifier with an inverse feedback

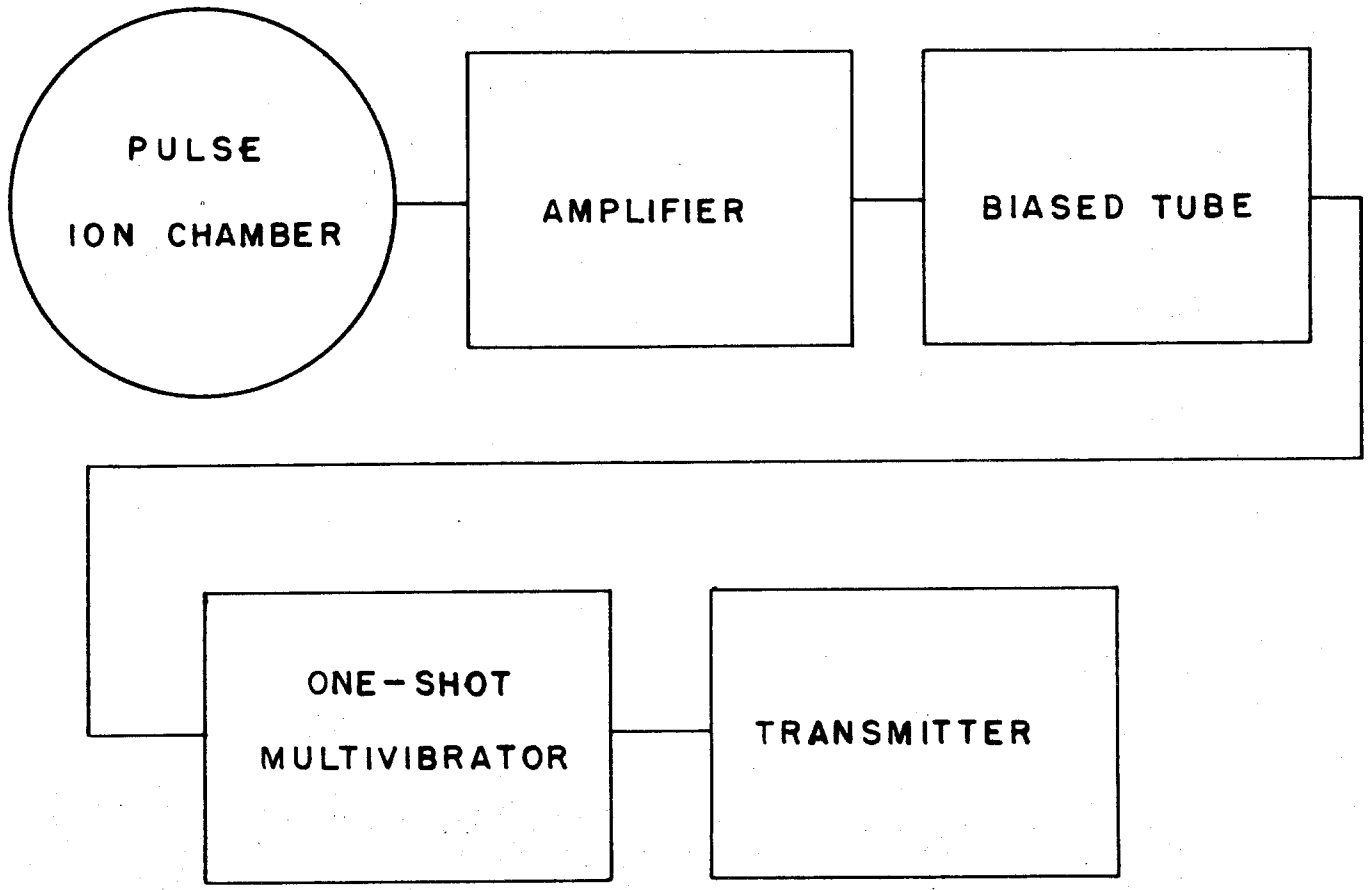

Figure 7a. Block diagram of electronics used in this experiment.

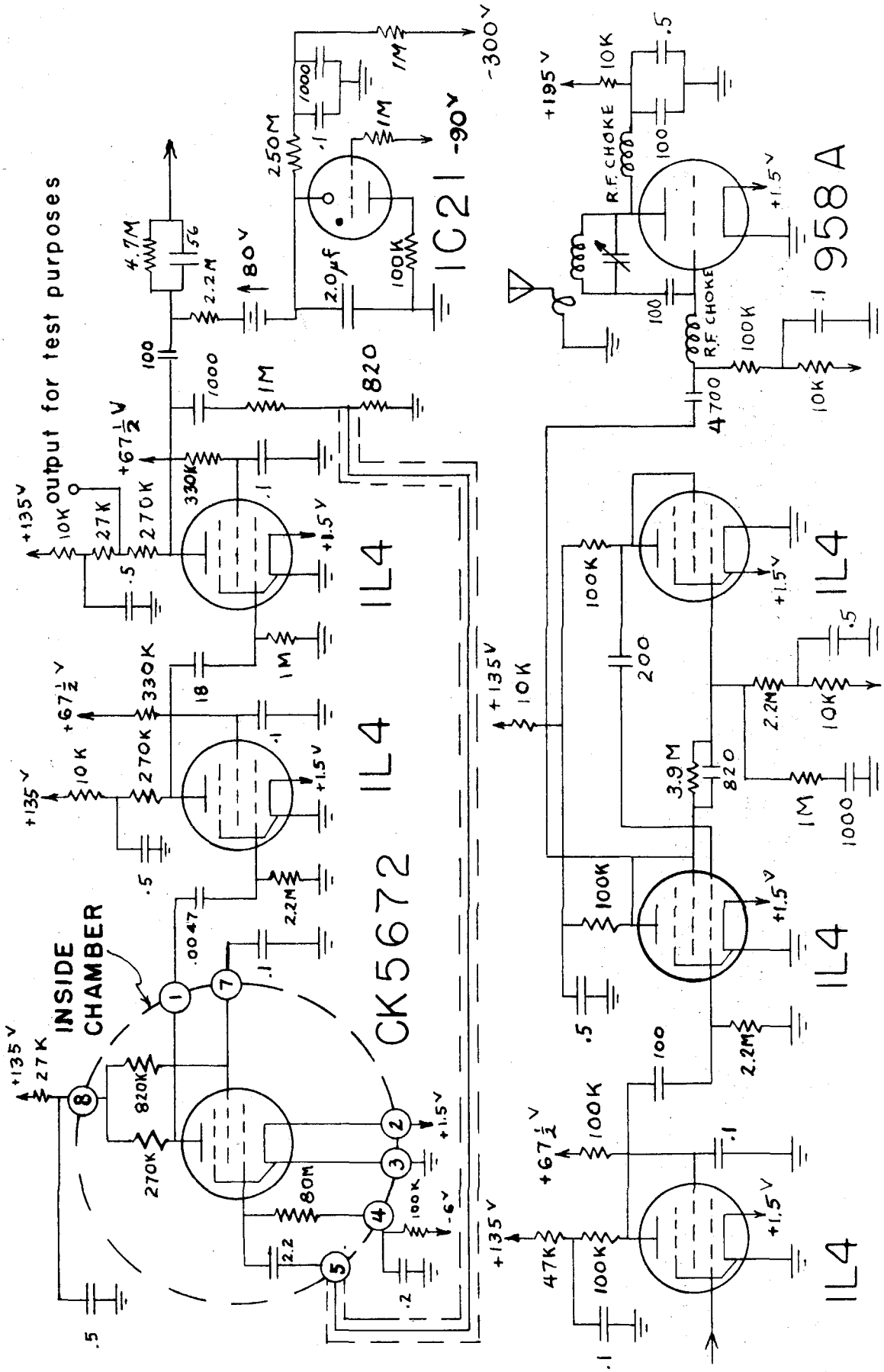

Figure 7. Schematic diagram of electronics used in this experiment.

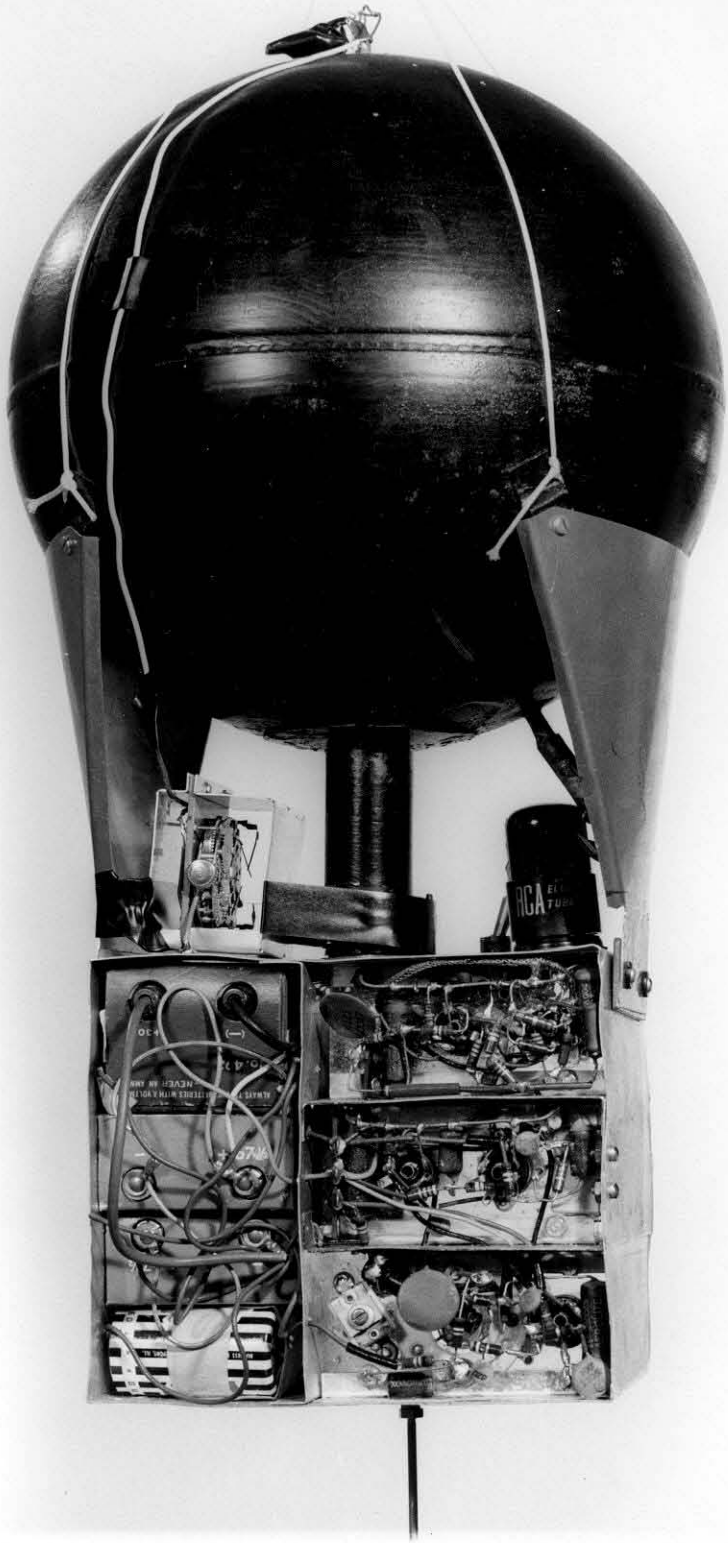

Figure 8. The assembled instrument batteried for a 4-hour flight. The lower half of the dipole antenna is the aluminum rod, part of which shows in the lower portion of the picture.

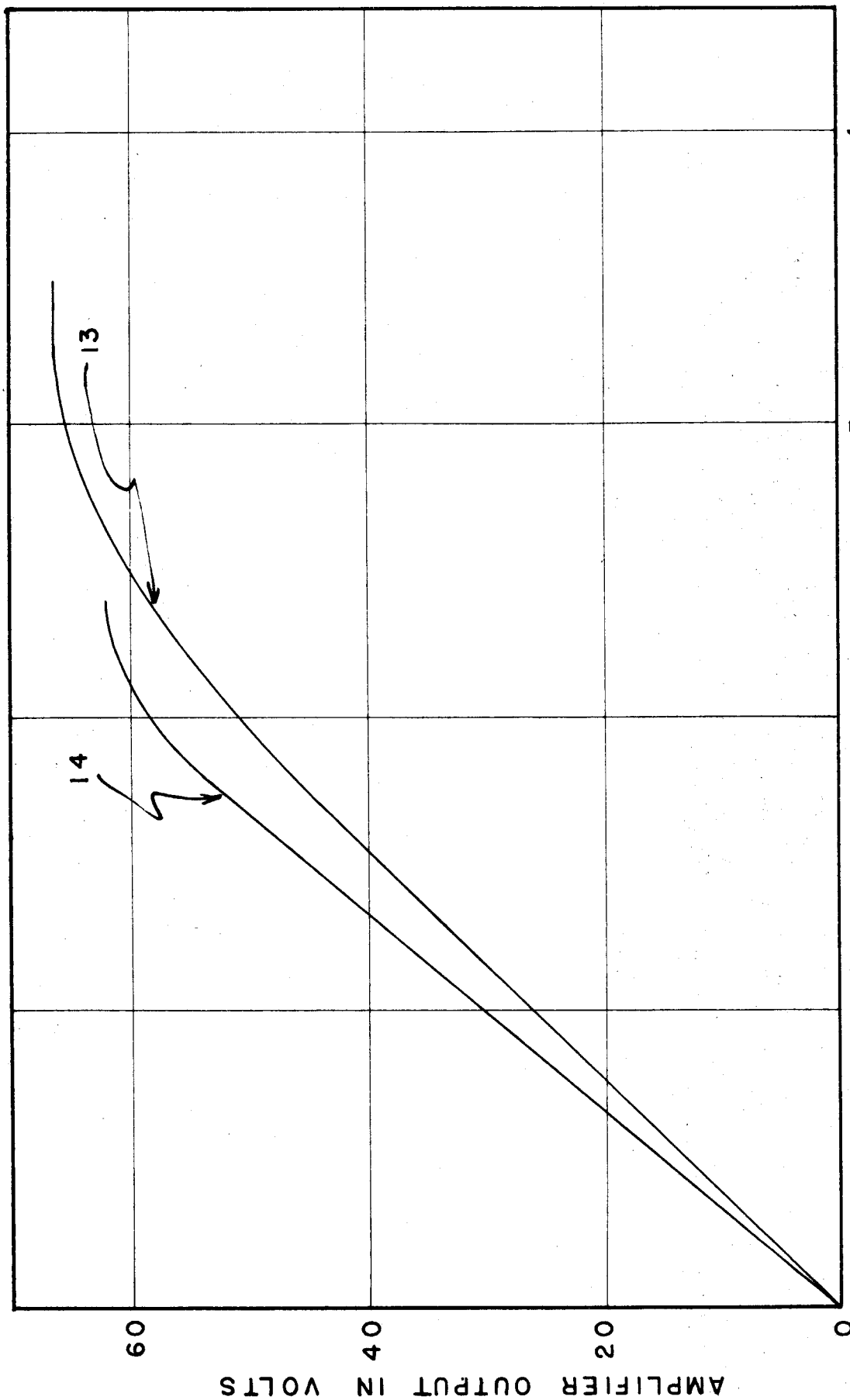

Figure 4. Linearity of the amplifiers for Chamber Nos. 13 and 14.

factor of about 15. The first tube is a CK 5672 subminiature, which was placed inside of the chamber to minimize the stray capacitance of the center electrode to ground. The circuit diagram of the electronics is shown in Figure 7b. The gain of the amplifiers was adjusted so that the pulse due to a Po α-particle was between 10 and 15 volts. The rise time of the amplifier was about 10 μsec. and the decay time was about 150 μsec. The amplifier noise voltage is about 2 percent a Po-α pulse. The collection time of the Po α-particle electrons was measured to be less than 5 μsec. so that the amplifier will amplify accurately pulses due to ionizing particles. A photograph of the assembled instrument is shown in Figure 8.

The linearity of both amplifiers used on the flight was checked by the following setup. A negative step function pulse was applied between the outer electrode of the chamber and the chassis, which was ground. Because of the capacitance between the center electrode and the outer electrode a negative step function pulse was induced on the center electrode simulating the input due to an ionizing particle passing through the chamber. The results shown in Figure 9 were obtained by varying the input and measuring by a fast oscilloscope the output of the amplifier. The output was taken off of the voltage divider (see Figure 7) so that the added capacitance of the oscilloscope probe would not affect the performance of the amplifier. It is seen that the ampli-

fier saturates at only about 60 volts. This condition can be improved by increasing the feedback resistors (1 megohm and 820Ω in Figure 7). The alternate possibility of connecting the 820Ω feedback resistor to the B^+ instead of ground did not work in this case. When this was done a low frequency oscillation of a few cycles/sec. developed because of feedback through the power supply.

The size of pulses at the output of the amplifier was determined by means of a 1L4 pentode biased beyond cutoff by a continuously varying sawtooth voltage. The biased tube only triggers the multivibrator for pulses larger than the size determined by the bias at the given time. Thus at the beginning of the sawtooth voltage when the bias is least negative almost every pulse triggers the multivibrator. As the bias voltage becomes increasingly negative, fewer and fewer pulses are passed. By this means the integral pulse height distribution of the pulses is obtained. The bias voltage goes through a complete cycle approximately every $3\frac{1}{2}$ minutes. The sawtooth voltage generator consists of the 2 μf oil capacitor, the 250 megohm resistor, and the 1C21 cold cathode tube connected as a relaxation oscillator (see Figure 7). The period of the relaxation oscillator was found to be constant to within about 5 percent during a flight so that this method measures voltages with an accuracy of at least 5 percent. The beginning and ending voltages of the sawtooth bias were determined by means of a very high impe-

dance electrostatic voltmeter. The voltage at any other part of the cycle was determined by assuming an exponential variation of voltage with time. This should be true if any leakage resistances are much larger than 250 megohms, which was found to be the case. Also, on one of the sawtooth generators, a direct measurement of the voltage vs. time was made with an electrostatic voltmeter, and it was found to have the expected exponential variation.

The output pulse from the biased tube is used to trigger a one-shot multivibrator. The multivibrator is used as a pulse shaper giving a square pulse about 1 millisecond long. A positive output is taken off of the multivibrator and used to start the 958 A transmitting tube oscillating. Normally the 958 A is biased beyond cutoff. The 958 A gives a C. W. pulse of about 1 millisecond duration at a frequency of about 155 megacycles per second.

The information from the sphere is thus telemetered down to the receiving station on the ground as a number of pulses. When the sawtooth bias voltage in the transmitter is at the beginning of its cycle many pulses per second are transmitted but as time progresses the frequency of pulses decreases. The sawtooth bias was adjusted so that near the end of the bias cycle no pulses at all are permitted to be transmitted. When the cycle ends and starts repeating again, many pulses per second are again transmitted. It is very

easy to tell from the record of the flight when the bias cycle started and ended and thus to determine the bias voltage at any time.

As the final calibration the overall linearity of the equipment was determined for various inputs on the grid of the CK5672 with the same input as used before but the time in the cycle when the instrument just stopped transmitting was now determined. The results for the equipment used in the flight are shown in Figures 10 and 11.

The transmitting antenna system was formed by the ion chamber and chassis acting as one half of an asymmetric dipole antenna and a 1/8" diameter aluminum rod as the other half (see Figure 8).

The signals from the transmitter were received on the ground by a yagi antenna connected to a superheterodyne receiver. The output of the receiver went to a scaler whose scaling factor could be changed from 8 to 4 to 2 to 1. The receiver output was controlled by a biased tube which could be adjusted to permit only signals larger than a certain value to trigger the scaler. The output of the scaler was used to trigger a recorder which put a mark on a moving paper tape. At the beginning of the bias cycle in the transmitter, when the frequency of pulses was high, the scaler was set to a scaling factor of 8. This scaling factor was then manually changed to the smaller values as the frequency of pulses decreased. Minute marks were automatically marked

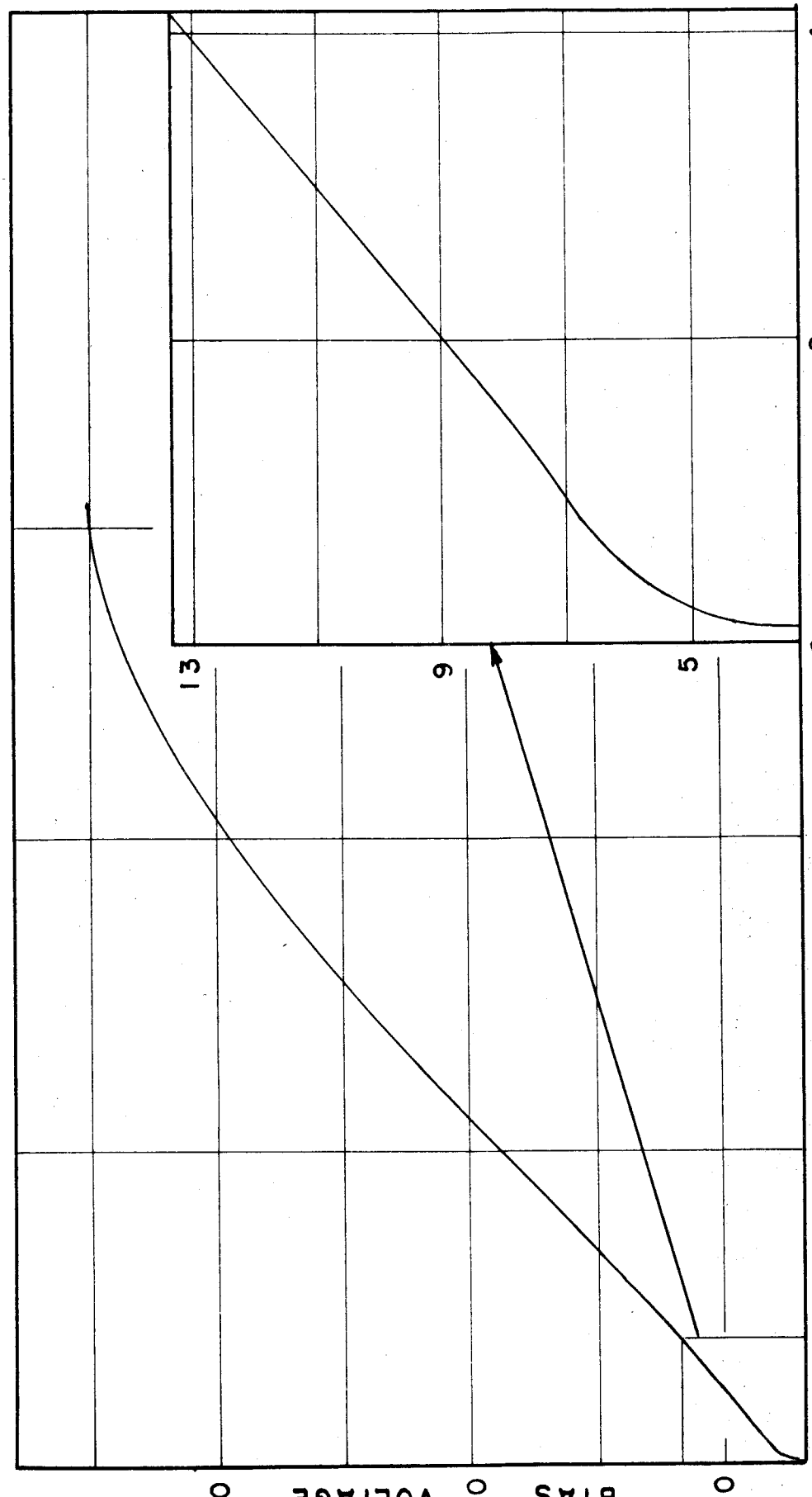

Figure 10. The overall linearity of the electronics of Chamber No. 13 for various inputs on the center electrode. The non-linearity in the lower portion of the curve is caused by the biased tube, and the non-linearity in the upper portion of the curve is caused by the saturation of the amplifier.

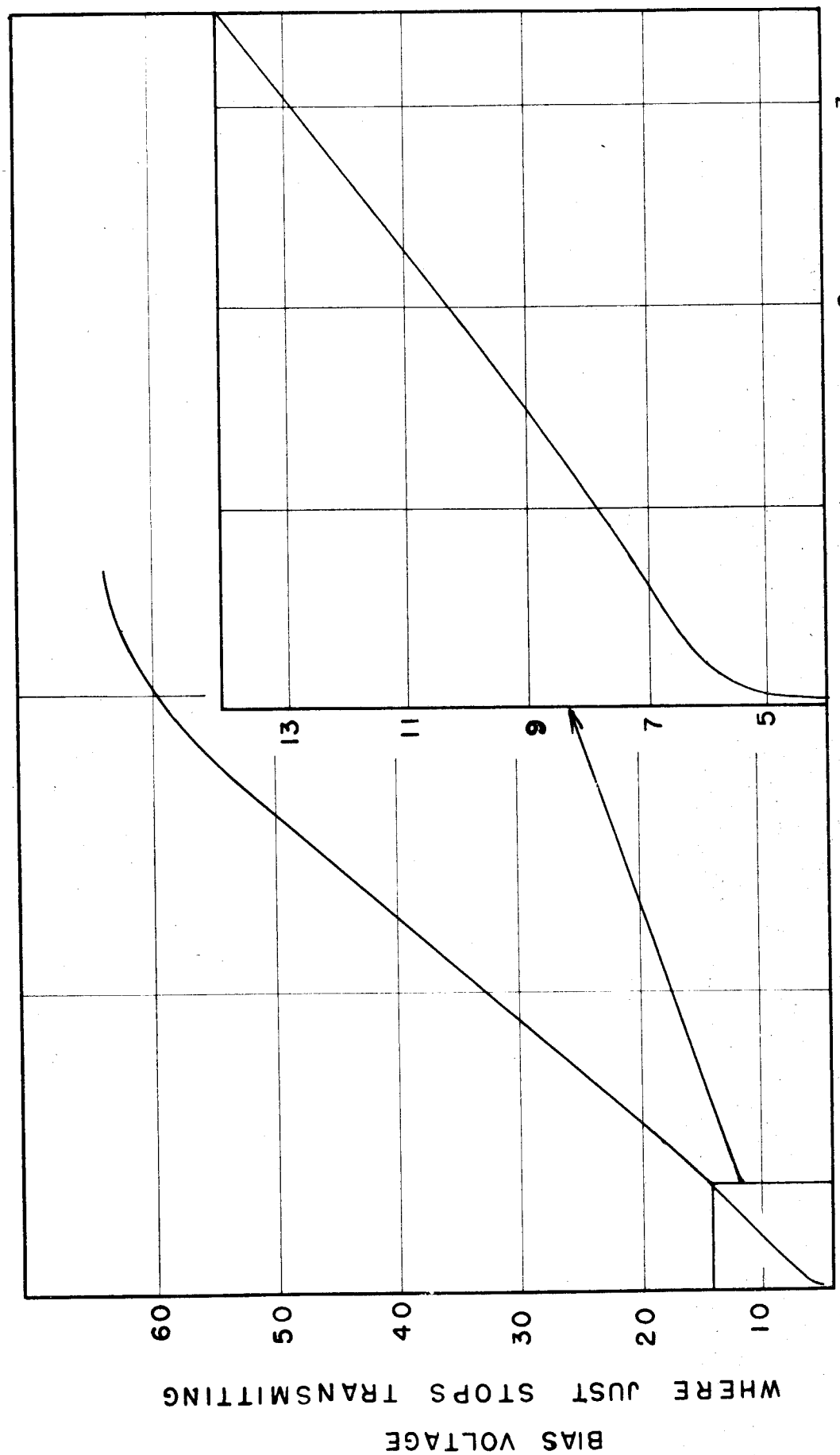

Figure 11. The overall linearity of the electronics of Chamber No. 14.

on the tape by a clock. The pressure record was obtained from the balloon contractor's instrument on the same balloon.

The method employed here of telemetering to ground the pulse size and number of pulses is different from other investigators; and it is worthwhile to compare this method with the others. Other methods have accomplished the same by using frequency modulation. The frequency of the carrier wave is modulated an amount that is a function of the pulse size.

The disadvantage of frequency modulation as far as balloon work is concerned is that the carrier frequency must be continuously transmitted. This causes much more power to be used in transmission, thus requiring more batteries and weight. The method employed in this experiment required the transmitter to be transmitting less than 1/1000 of the time. Coor,[9] using frequency modulation, required 30 lbs. of equipment to accomplish essentially the same that was done by the 14 pounds of equipment of this experiment.

The method used in this experiment is also much simpler than frequency modulation. It requires fewer tubes and circuitry and consequently has less probability of going wrong during a flight.

However, as seems to be true in Nature, one does not gain something for nothing. Where one gains in simplicity and weight one loses in the amount of information one can

transmit per unit time. With frequency modulation the pulse size may be transmitted with each pulse. With the method employed in this experiment not every pulse is transmitted, and when it is, only the information that it is larger than a certain value is transmitted with it. This has the effect of requiring much longer balloon flights to obtain the same statistics as obtained when frequency modulation is used.

EXPERIMENT

In designing an experiment wherein pulse ionization chambers are used to measure cosmic rays, it is important to determine the effect of nuclear stars, which can give pulses the size of heavy primary cosmic-ray particles. In the present experiment this was done by sending up on the same balloon two pulse ionization chambers which were identical in every respect except for the argon pressure inside the chambers. Sphere No. 14 had 3.17 atmospheres of argon, and Sphere No. 13 had 1.48 atmospheres of argon. Low energy evaporation particles from nuclear stars will stop in both chambers and give approximately the same pulse sizes, but cosmic-ray particles that pass completely through will give pulses proportional to the pressure. By comparing the statistically related counting rates of the two chambers it is possible to estimate the effect of nuclear stars.

A skyhook balloon flight was made October 20, 1954, at South St. Paul, Minnesota ($\lambda = 55^{\circ}$ geomagnetic latitude). The balloon was launched at 7:06 A. M., reached altitude at about 8:40 A. M., and stayed at a nearly constant altitude of 95,000 feet until 2:35 P. M., when the instruments were cut loose. The time-pressure curve is shown in Figure 12. The atmospheric pressure during the level portion of the flight varied between 13.8 gm/cm^2 and 14.9 gm/cm^2. It is

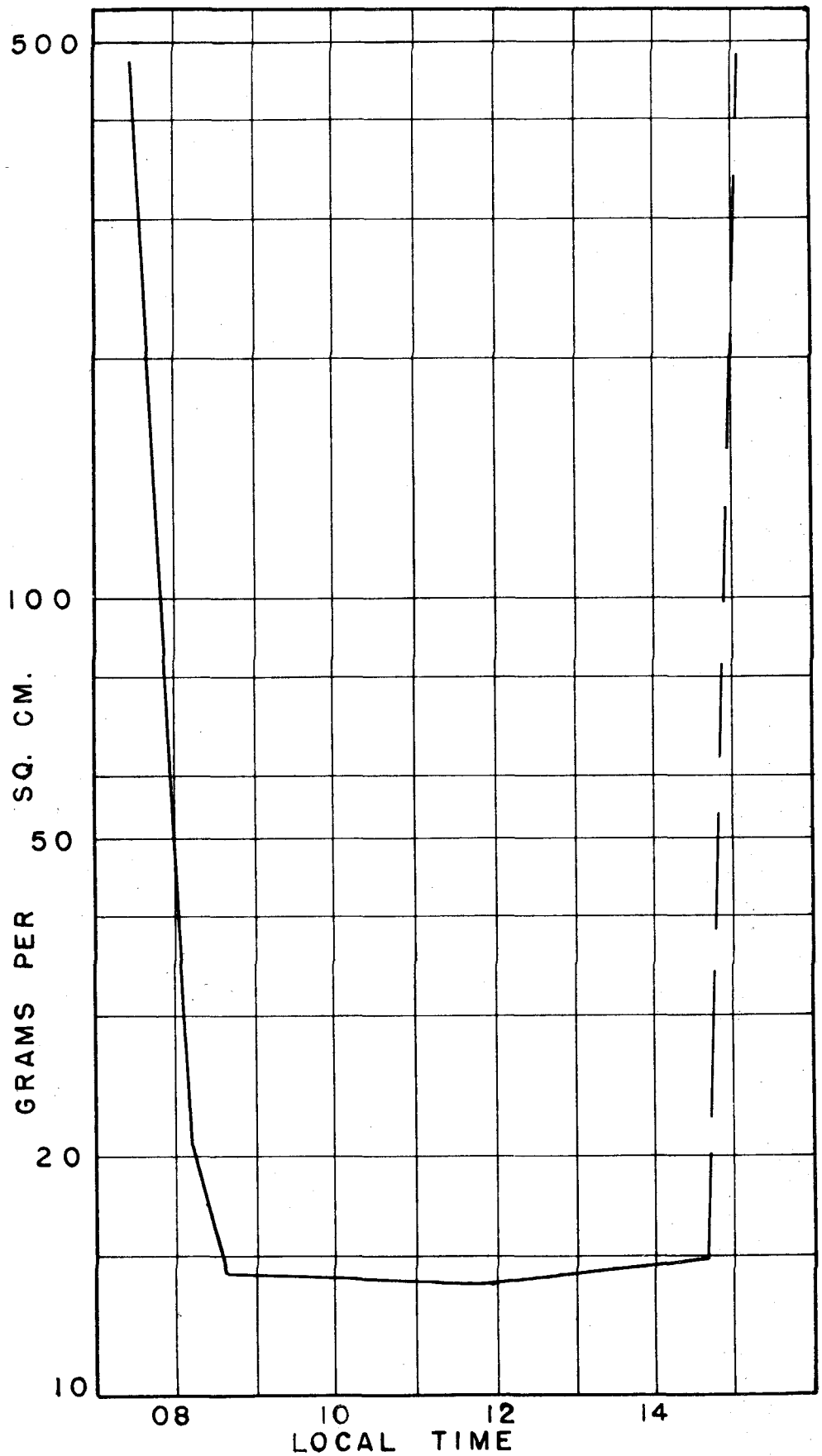

Figure 12. The time-pressure curve of the balloon flight of this experiment. The balloon was launched Oct. 20, 1964.

accurate enough to consider that the instrument was, during the level portion of the flight, at the average depth of 14.3 gm/cm^2. The wall thickness of the chamber is about .5 gm/cm^2 of steel. We will take the counting rate of the chamber as a measure of the cosmic rays at a depth of 15 gm/cm^2, since cosmic ray particles have to traverse both the atmosphere and the chamber wall before being detected. The two instruments were separately wrapped with 5 layers of glass wool insulation, covered with cellophane, and placed inside a bamboo cage which was covered with transparent cellophane and white paper so that about 50 percent of its area was transparent to sunlight. The cage was used to give a greenhouse effect and keep the temperature of the instruments in the operating region. One instrument was placed just below the neck of the balloon, and the other one about 15 feet below it. The other equipment on the balloon was placed far enough below both instruments so that nuclear interactions produced in them did not have any appreciable effect on the counting rate of the chambers. With the aforementioned precautions it is believed that practically all pulses produced in the chambers were from cosmic rays or nuclear stars formed in the chamber wall and in the chamber gas.

The two instruments were more than amply batteried for the 8-hour duration of the flight. In fact, when the two instruments were recovered the next day, the batteries were

still not completely run down. When fully wrapped and batteried for the eight-hour flight, each instrument weighed 14 pounds.

RESULTS

In reducing the data, each bias voltage cycle was divided into the voltage intervals shown in Tables I and II. The large number of voltage intervals permits a more detailed determination of the finer structure in the integral pulse height curve. The bias voltage of No. 13 varied from $-3.7 \pm .2$ volts to $-83.5 \pm .4$ volts, while the bias voltage of No. 14 varied from $-6.8 \pm .2$ volts to $-92 \pm .5$ volts. These bias voltages correspond to pulse sizes from $.24 \pm .02$ volts for No. 13 and $1.8 \pm .3$ volts for No. 14, to past amplifier saturation for both spheres. The counting rate of No. 13 at the beginning of the bias cycle was too high to measure with the equipment, and it is neglected. However, this very high counting rate affects the voltage measured by the bias voltage and requires a correction. When the grid of the biased 1L4 tube at the output of the amplifier is driven positive, the resultant grid current gives an additional charge to the 2 μf capacitor and changes the bias voltage from the calibration value. This grid current is only appreciable when the counting rate is very high and affects only No. 13. This correction was calculated and the necessary corrections are indicated in

Table I. Integral pulse height distribution of the counting rate in Chamber No. 13 at $\lambda = 55^{\circ}$ and at 15 gm/cm^2 atmospheric pressure. The pulse sizes given have not been multiplied by 1.24 as is done in Figure 13. All errors are standard errors.

Voltage Interval No.	Pulse Ht. Limits in Volts	Grid Current Correction for Middle of Interval	True Pulse Ht. Voltage Limits	Total No. of Counts	Counts/ Second	Dead-time Correction (Add)	Po-Background Correction (Subtract)	True Counts/ Sec.
1	.34-.38	.11	.45-.51	642	55.4±2.2	12.2	9.6	58.0±2.2
2	.38-.46	.14	.51-.62	612	40.8±1.7	6.3	8.6	38.5±1.7
3	.46-.58	.18	.62-.82	648	29.8±1.2	3.6	6.0	27.4±1.2
4	.58-.79	.30	.82-1.15	533	19.5±.8	1.5	1	20.0±.8
5	.79-1.22	.42	1.15-1.70	484	14.0±.6	.8	-	14.8±.6
6	1.22-1.9	.54	1.70-2.5	240	10.3±.7	.4	-	10.7±.7
7	1.9-2.8	.67	2.5-3.4	219	7.5±.5	.2	-	7.7±.5
8	2.8-3.8	.6	3.4-4.4	137	4.7±.4	.1	-	4.8±.4
9	3.8-4.5	.6	4.4-5.1	114	5.0±.5	.1	-	5.1±.5
10	4.5-5.1	.6	5.1-5.7	91	3.91±.41	.06	-	3.97±.41
11	5.1-5.7	.6	5.7-6.3	87	2.96±.32	.04	-	3.00±.32
12	5.7-6.4	.6	6.3-7.0	63	2.38±.30	-	-	2.38±.30
13	6.4-7.1	.6	7.0-7.7	58	2.31±.30	-	-	2.31±.30
14	7.1-8.1	.6	7.7-8.7	131	2.66±.23	-	-	2.66±.23
15	8.1-9.3	.6	8.7-9.9	76	1.72±.20	-	-	1.72±.20
16	9.3-10.4	.6	9.9-11.0	82	1.70±.19	-	-	1.70±.19
17	10.4-11.7	.6	11.0-12.3	97	1.23±.13	-	-	1.23±.13
18	11.7-13.3	.6	12.3-13.9	119	1.07±.10	-	-	1.07±.10
19	13.3-14.7	.6	13.9-15.3	123	.92±.08	-	-	.92±.08
20	14.7-16.4	.6	15.3-17.0	159	.88±.07	-	-	.88±.07

Table I. (continued)

Voltage Interval No.	Pulse Ht. Limits in Volts	Grid Current Correction for Middle of Interval	True Pulse Ht. Voltage Limits	Total No. of Counts	Counts/ Second	Dead-time Correction (Add)	Po-Back-ground Correction (Sub-tract)	True Counts/ Sec.
21	16.4-17.5	.6	17.0-18.1	122	.89±.08	-	-	.89±.08
22	17.5-18.8	.6	18.1-19.4	75	.61±.07	-	-	.61±.07
23	18.8-20.0	.6	19.4-20.6	79	.49±.055	-	-	.49±.055
24	20.0-21.3	.6	20.6-21.9	86	.58±.063	-	-	.58±.063
25	21.3-22.7	.6	21.9-23.3	58	.37±.048	-	-	.37±.048
26	22.7-24.0	.6	23.3-24.6	60	.38±.049	-	-	.38±.049
27	24.0-25.5	.6	24.6-26.1	62	.36±.046	-	-	.36±.046
28	25.5-27.0	.6	26.1-27.6	57	.31±.041	-	-	.31±.041
29	27.0-28.8	.6	27.6-29.4	61	.28±.036	-	-	.28±.036
30	28.8-30.5	.6	29.4-31.1	39	.19±.030	-	-	.19±.030
31	30.5-32.2	.6	31.1-32.8	54	.24±.033	-	-	.24±.033
32	32.2-34.8	.6	32.8-35.4	55	.175±.024	-	-	.175±.024
33	34.8-37.0	.6	35.4-37.6	48	.172±.025	-	-	.172±.025
34	37.0-39.4	.6	37.6-40.0	34	.192±.033	-	-	.192±.033
35	39.4-42.3	.6	40.0-42.9	53	.159±.022	-	-	.159±.022
36	42.3-44.9	.6	42.9-45.5	32	.116±.021	-	-	.116±.021
37	44.9-47.9	.6	45.5-48.5	36	.113±.022	-	-	.113±.022
38	47.9-50.6	.6	48.5-51.2	34	.118±.020	-	-	.118±.020
39	50.6-53.7	.6	51.2-54.3	30	.106±.019	-	-	.106±.019
40	53.7-58.4	.6	54.3-59.0	23	.063±.013	-	-	.063±.013
41	58.4-64.3	.6	59.0-64.9	19	.047±.012	-	-	.047±.012
42	64.3-100	.6	64.9-101	13	.0135±.006	-	-	.0135±.006

Table II. Integral pulse height distribution of the counting rate in Chamber No. 14 at $\lambda = 55^{\circ}$ and at 15 gm/cm^2. All errors are standard errors.

Voltage Interval No.	Pulse Ht. Limits in Volts	Total No. of Counts	Counts/ Sec.	Deadtime Correction (Add)	True Counts/ Sec.
1	2.0-2.8	864	31.6±1.1	2.5	34.1±1.1
2	2.8-3.7	617	22.0±.9	1.2	23.2±.9
3	3.7-4.5	607	16.8±.7	.7	17.5±.7
4	4.5-5.5	640	13.0±.5	.4	13.4±.5
5	5.5-6.1	284	10.6±.6	.3	10.9±.6
6	6.1-6.8	265	10.0±.6	.3	10.3±.6
7	6.8-7.6	323	8.65±.48	.19	8.84±.48
8	7.6-8.3	301	8.05±.47	.16	8.21±.47
9	8.3-9.1	261	6.95±.43	.12	7.07±.43
10	9.1-10.1	281	6.58±.40	.11	6.69±.40
11	10.1-11.2	315	5.75±.32	.08	5.83±.32
12	11.2-12.5	310	4.50±.26	.05	4.55±.26
13	12.5-13.8	265	4.24±.26	.04	4.28±.26
14	13.8-15.3	391	3.50±.18	.03	3.53±.18
15	15.3-16.6	360	3.07±.16	.02	3.09±.16
16	16.6-18.0	401	2.76±.14	.02	2.78±.14
17	18.0-19.0	210	2.18±.15	.01	2.19±.15
18	19.0-20.0	204	1.99±.14	-	1.99±.14
19	20.0-21.2	261	2.01±.13	-	2.01±.13
20	21.2-22.4	217	1.83±.12	-	1.83±.12
21	22.4-23.7	249	1.57±.10	-	1.57±.10
22	23.7-25.2	260	1.37±.09	-	1.37±.09
23	25.2-26.5	184	1.31±.10	-	1.31±.10
24	26.5-28.1	197	1.11±.08	-	1.11±.08
25	28.1-30.0	221	1.03±.07	-	1.03±.07

Table II. (continued)

Voltage Interval No.	Pulse Ht. Limits in Volts	Total No. of Counts	Counts/ Sec.	Deadtime Correction (Add)	True Counts/ Sec.
26	30.0-31.8	207	.95±.066	-	.95±.066
27	31.8-33.5	165	.855±.067	-	.855±.067
28	33.5-36.0	242	.76±.048	-	.76±.048
29	36.0-38.3	214	.72±.049	-	.72±.049
30	38.3-40.8	200	.60±.043	-	.60±.043
31	40.8-43.3	203	.57±.040	-	.57±.040
32	43.3-45.6	180	.53±.039	-	.53±.039
33	45.6-47.9	145	.43±.036	-	.43±.036
34	47.9-50.0	130	.374±.033	-	.374±.033
35	50.0-52.2	107	.302±.029	-	.302±.029
36	52.2-55.7	141	.302±.025	-	.302±.025
37	55.7-60.0	144	.304±.025	-	.304±.025
38	60.0-63.5	108	.224±.021	-	.224±.021
39	63.5-81.3	102	.204±.020	-	.204±.020

Table I. In calculating this correction the experimentally determined fact was used that whenever a pulse was transmitted, some sort of feedback occurred which produced at the output of the amplifier a pulse saturating the amplifier.

The counts shown in Tables I and II are the total counts in each voltage interval summed over bias voltage cycles. For a portion of the balloon flight the received signal was very weak due to the balloon's being almost straight overhead, placing the receiving equipment near the radiation node of the vertical dipole transmitting antenna. The information received during this time was unreliable because pulses were missed and interspersed with noise pulses. This portion of the record was discarded. By looking at the distribution of pulses along the tape during a cycle, it is possible in many cases to determine if the data are good by noting if the frequency of pulses decreases from the beginning of the cycle to the end. Whenever it was evident that some pulses were missed at the beginning of a cycle, the cycles were not counted. As a check on the self-consistency of the data, the data for the portion of the flight where the signal was very strong and there was great confidence that the records were correct were compared with the total data, and the results were found to be statistically consistent. By counting the number of pulses that were recorded during the last portion of the cycles, where no signals are transmitted, it was found that noise was completely negligible.

A check on the constancy of the gain of the ion chamber amplifier and the overall operation of the transmitting and receiving equipment during the flight was afforded by the Po-α pulses in the ion chamber that were turned on for a cycle every 15 minutes. Measuring the voltage in the cycle where the Po-α pulses were just cut off showed that during the flight the gain of the amplifiers changed by less than could be measured by this method, namely less than 5 percent. Measuring the increased counting rate due to the Po-α pulses showed that during the flight the transmitting and receiving equipment were operating satisfactorily.

The calibration of each chamber was afforded by the Po-α pulses. Po α-particles have an energy of 5.3006 Mev, (10) and, since they stop in the chamber, they lose that amount of energy. From the integral pulse height curve for Po- α's shown in Figure 6, it is seen that the Po α-particles do not give a unique pulse, but rather the pulse size varies. This was interpreted as being due to the fact the Po α-particles are not collimated, and each will move in a direction with a different potential factor. Also, some of the pulses are due to α-particles that have been backscattered from the foil. For certain trajectories for the α-particles, namely those near the wall, the potential factor will be very nearly one. Thus the maximum pulse should correspond to 5.30 Mev energy loss and a potential factor of one.

On the basis of the maximum Po-α pulse, the pressures

Table III. Characteristics of the two pulse ionization chambers used in this experiment.

Chamber No.	Diam.	Density of Argon	$S_{Po-\alpha}$, max. pulse Due to Po-α	Average Chamber Wall Thickness
13	25.5 cm.	5.20 g/ℓ	10.5±.3	.47 gm/cm^2
14	25.5 cm.	2.43 g/ℓ	13.0±.4	.47 gm/cm^2

in the two chambers, and the fact that a singly charged minimum ionizing particle loses the average energy of 1.49 Mev/gm - cm^2 in argon, it is possible to calculate the pulses due to a particle of charge Z. The pertinent data are given in Table III. The average pulse produced by a minimum ionizing particle of charge Z when traversing that portion of the chamber that gives the maximum pulses [see Equation 6a] is

$$\frac{S_{max}^{min}}{S_{Po-\alpha}} = \frac{Z^2 \ .757 \times 25.5 \times 1.49 \times 10^{-3} \ p}{5.30} \quad , \quad (7.1)$$

where .757 is the potential factor calculated in Equation 7, 25.5 cm is the diameter of the spheres, p is the density of the argon in the chambers given in Table III, S_{max}^{min} is the maximum average pulse due to a minimum ionizing particle of charge Z, and $S_{Po-\alpha}$ is the maximum pulse due to Po α-particles given in Table III.

Since in this experiment it is important to know accurately the ratio of the densities in each sphere, after the flight the density of argon in the recovered instruments was measured by weighing. The results were found to agree within 1 percent with the measurements made when the spheres were first filled.

In the above discussion it is assumed[3,4] that the energy of formation of an ion pair is independent of the energy and type of the ionizing particle, which implies that

Table IV. The maximum average pulse size in Chamber No. 14 caused by minimum ionizing particles, S_{max}^{min} (1.0 on abscissa of Figures 19 and 20).

Particle Charge	S_{max}^{min} for Chamber No. 14
1	.37 volts
2	1.47
3	3.30
4	5.87
5	9.17
6	13.2
7	18.0
8	23.5
9	29.8
10	36.6
11	44.5
12	53.0
13	62.0
14	72.0
15	82.5

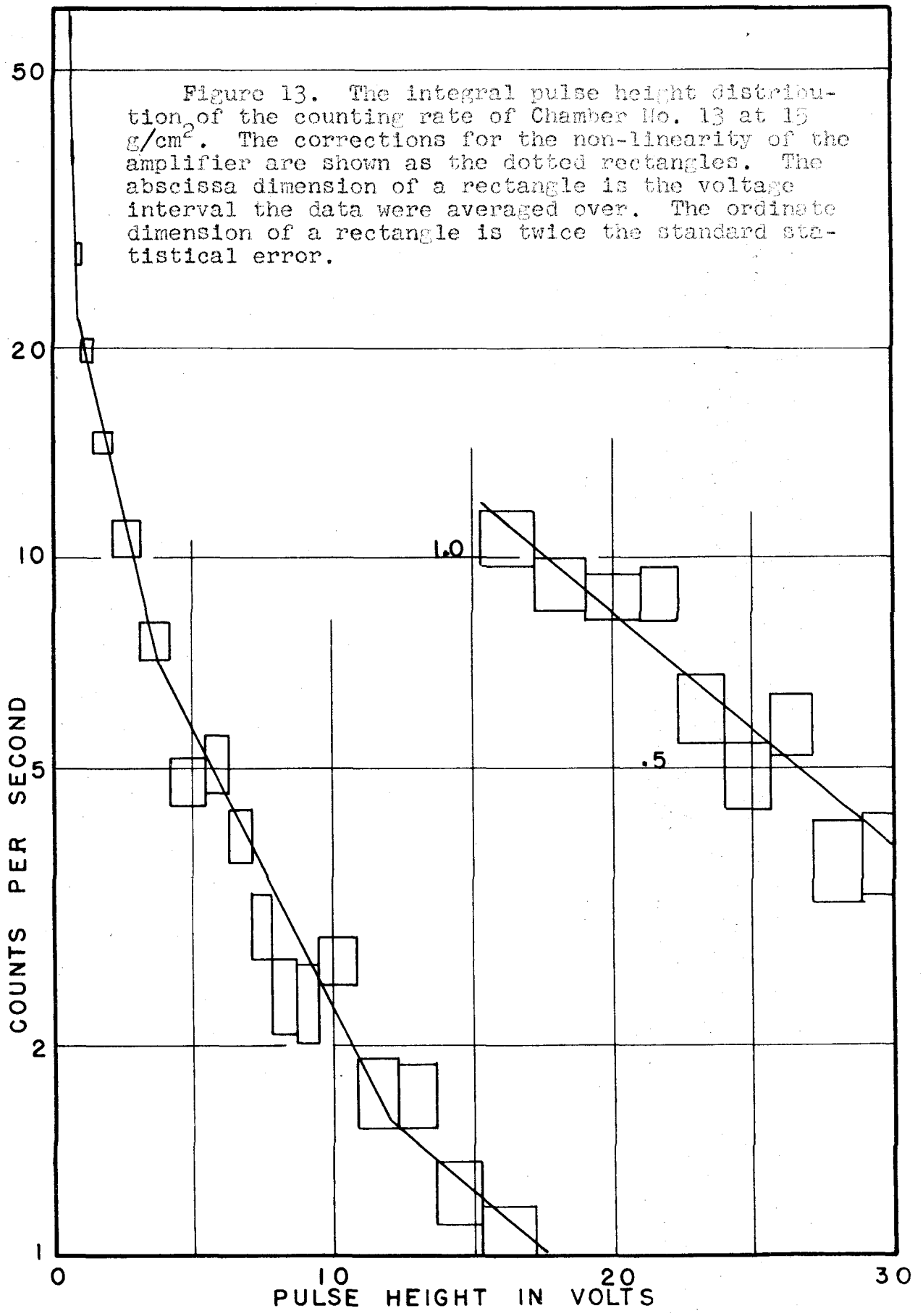

Figure 13. The integral pulse height distribution of the counting rate of Chamber No. 13 at 15 g/cm^2. The corrections for the non-linearity of the amplifier are shown as the dotted rectangles. The abscissa dimension of a rectangle is the voltage interval the data were averaged over. The ordinate dimension of a rectangle is twice the standard statistical error.

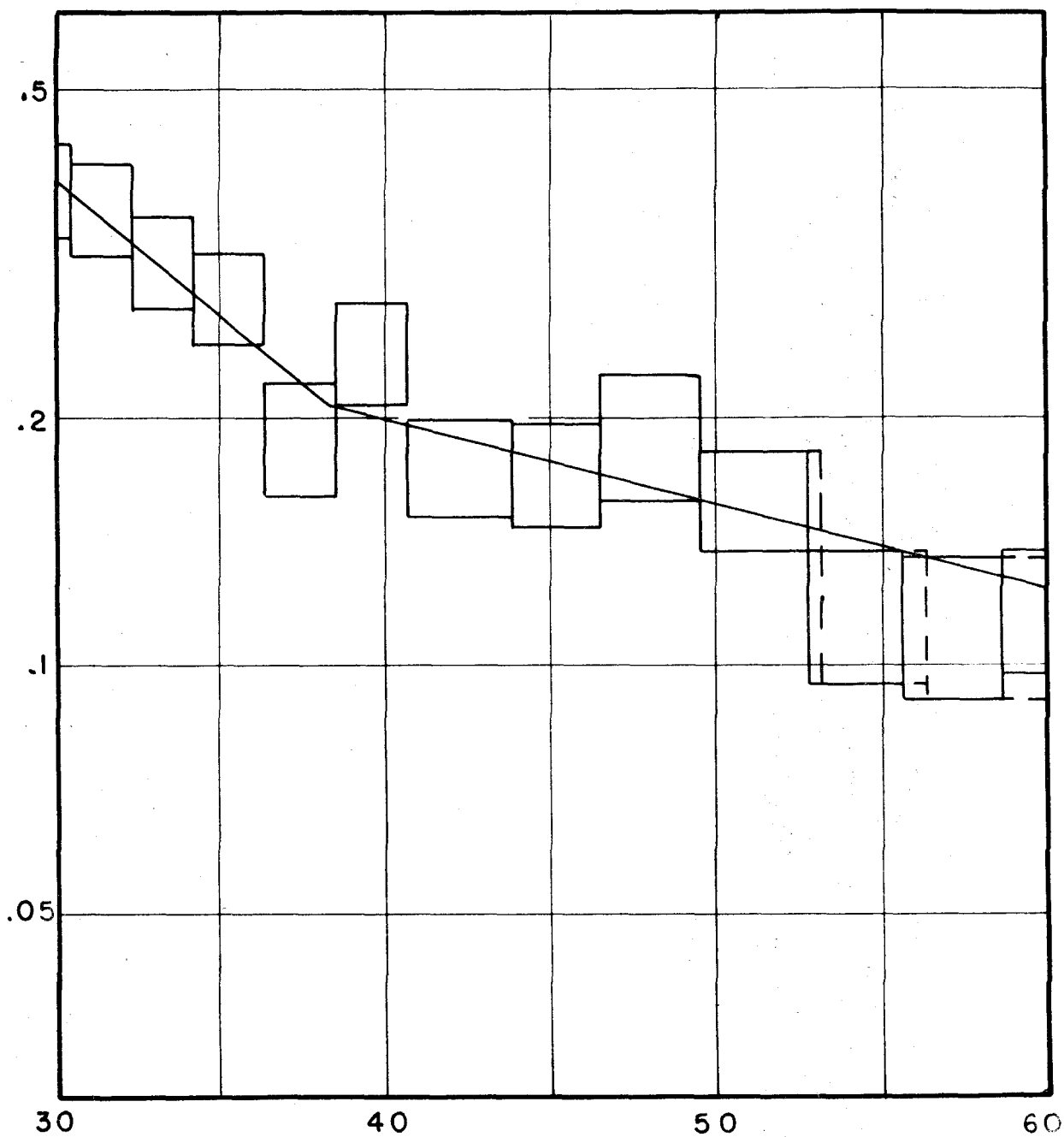

Figure 13. (continued)

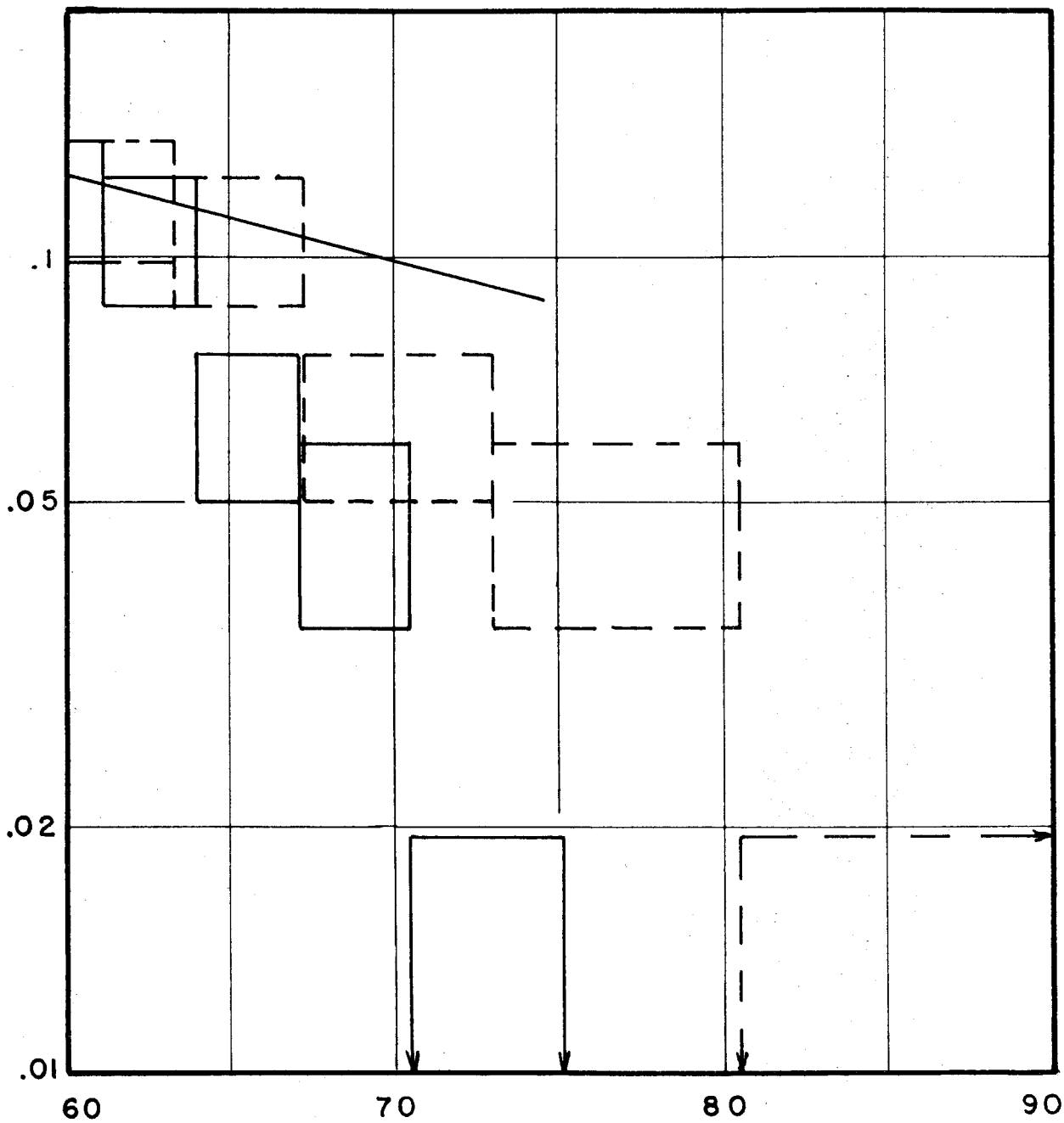

Figure 13. (continued)

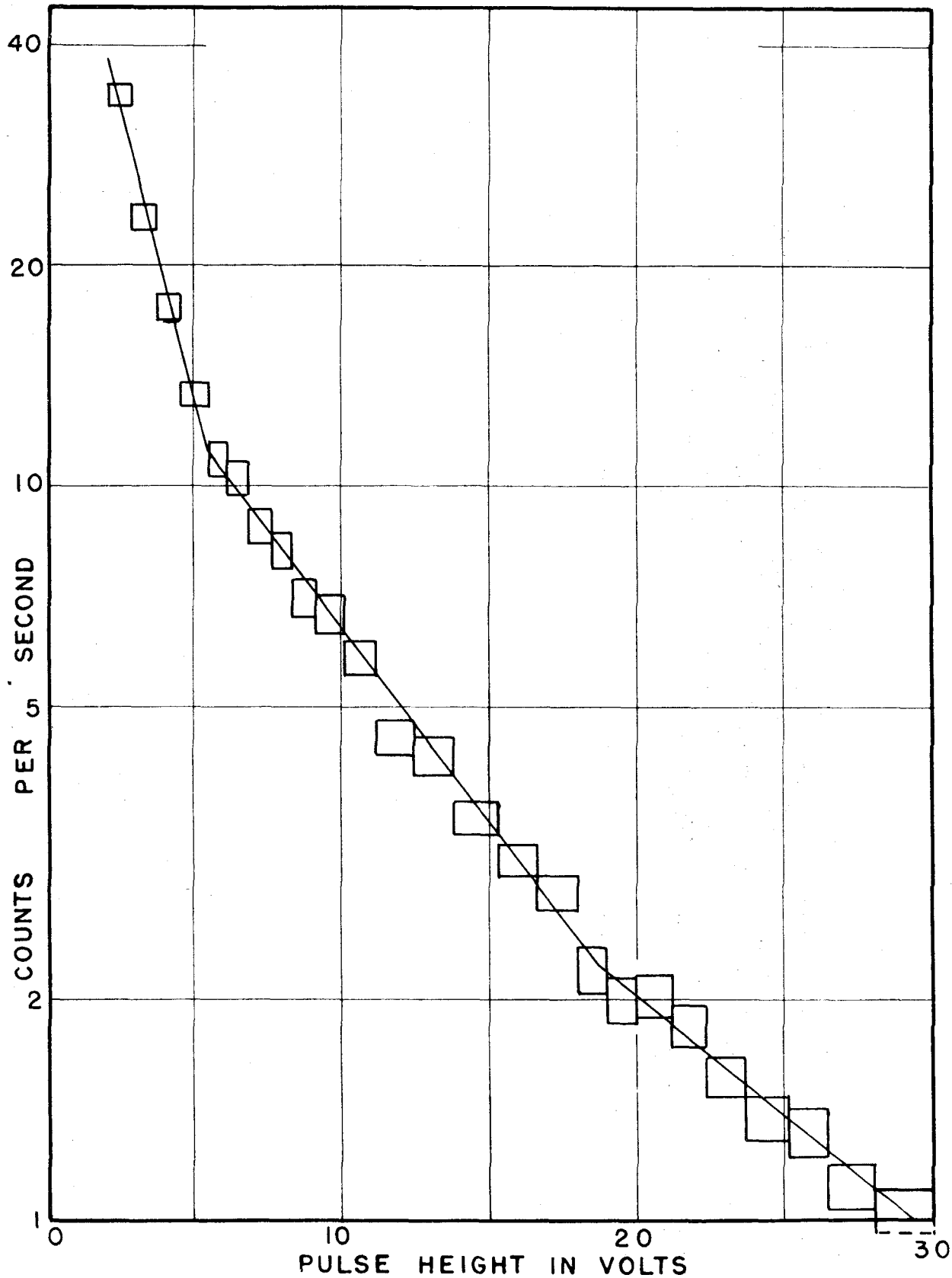

Figure 14. The integral pulse height distribution of the counting rate of Chamber No. 14 at 15 g/cm^2. The corrections for the non-linearity of the amplifier are shown as the dotted rectangles.

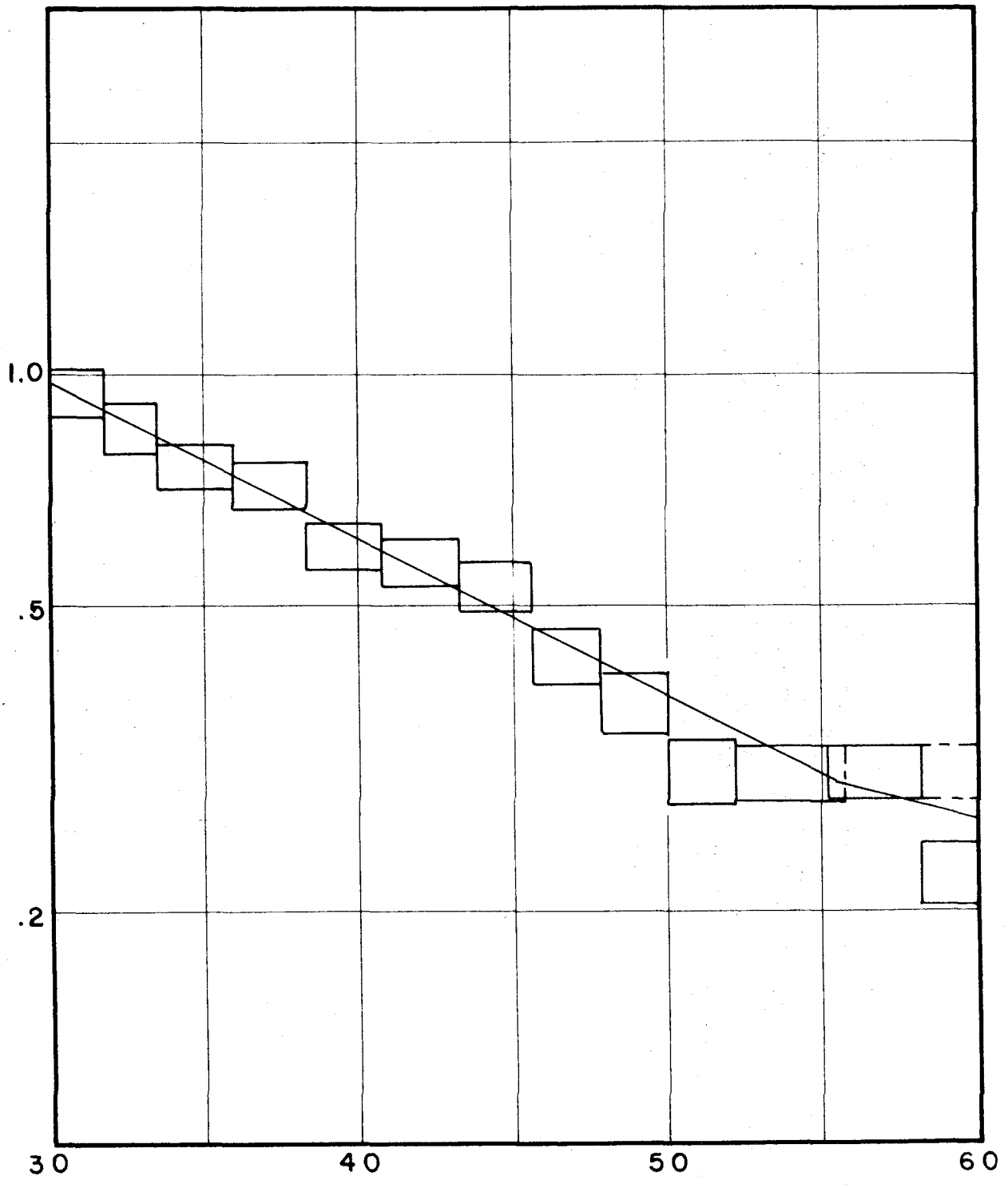

Figure 14. (continued)

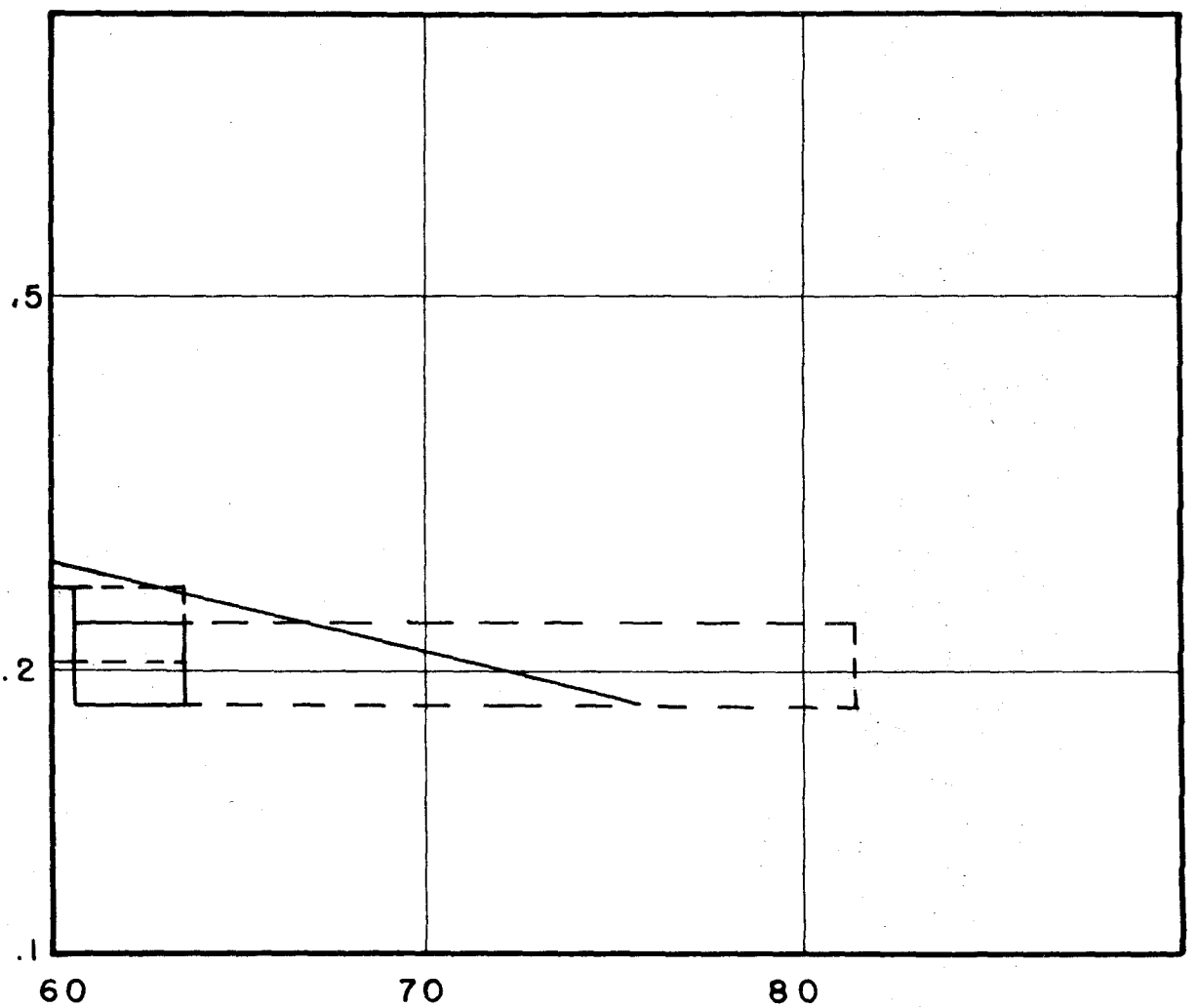

Figure 14. (continued)

the number of ion pairs formed is proportional to the energy loss of the particle.

S_{max}^{min} is shown in Table IV for Chamber No. 14 for various charged particles.

The counting rates corrected for dead time, Po-α background for Chambers No. 13 and No. 14, and non-linearity of the amplifiers are plotted in Figures 13 and 14. The voltage scale of No. 13 was multiplied by 1.24 so that $S_{Po-\alpha}$ for No. 13 will equal that of No. 14, 13 volts. The dead time for No. 13 was 4 milliseconds and for No. 14, 2.5 milliseconds. The range of the Po α-particles in Sphere No. 13 (the chamber with 1.48 atmospheres of argon) was great enough that not all of the electrons were collected back on the Po-α electrode when the Po-α's were turned off, even though the electrode was then connected to +195 volts. This produced a background of pulses that was measured on the ground and has to be subtracted out from the flight data. The range of the Po α-particles in No. 14 was short enough that this effect did not occur when the Po-α electrode was turned off by grounding it, and consequently no Po-α background correction is needed for No. 14. The correction for non-linearity of the amplifiers was performed using Figures 10 and 11.

BACKGROUND CORRECTION

The counting rate of a pulse ionization chamber adjusted to measure the heavy primaries is caused by the following:

(a) Heavy cosmic-ray primaries

(b) Fragments of heavy primary particles

(c) Nuclear star evaporation particles

(d) Slow secondary protons produced in the collisions of the primary and secondary flux with the atmosphere and material surrounding the chamber

(e) Slow α-particles

(f) Electron shower particles

(g) Pileup of small pulses producing a detectable pulse

In order to determine the contribution of the heavy primary cosmic-ray flux and its fragments to the chamber counting rate, we must be able to determine the contribution of items (c) through (g), the undesired background.

Nuclear Stars

In the first part of this section some pertinent facts about nuclear stars will be briefly reviewed,[11] and then a calculation will be performed to estimate the effect of stars on the counting rate of the chambers.

Data on nuclear stars produced in emulsions by neutrons

or protons show that the star-prong tracks can be divided into three classes: thin tracks, grey tracks, and black tracks. Thin tracks are defined as those with a grain density between 1 and 1.4 times minimum grain density, g_{min}. Grey tracks have a grain density 1.4 to 6.8 $g_{min.}$, and black tracks have grain densities greater than 6.8 $g_{min.}$. The limit of 6.8 $g_{min.}$ corresponds to a proton of 25 Mev. The limit of 1.4 $g_{min.}$ corresponds to protons of 500 Mev and π-mesons of 80 Mev.

The thin tracks, also called shower particles, are composed mostly of π-mesons, the rest being mainly protons. The grey tracks are mostly protons, the rest being mesons. About 2/3 of the black tracks are caused by low energy singly charged particles (80 to 90 percent are protons, the remainder being deuterons and tritons), and 1/3 are produced by multiply charged particles of which about 80 to 90 percent are α-particles. The black tracks are emitted uniformly in all directions. The energy distribution of black tracks from stars with 3 to 6 black prongs is shown in Figure 15.

On the average there are about $2\frac{1}{2}$ to 3 times as many black as grey tracks. Most stars have a small number of prongs and the number of stars falls off rapidly as the number of prongs increases. The evidence indicates that at 94,000 feet and $\lambda = 54^{o}$ [12] about 5/8 of the total stars produced in emulsions have 5 or less black tracks (7 or less total prongs).

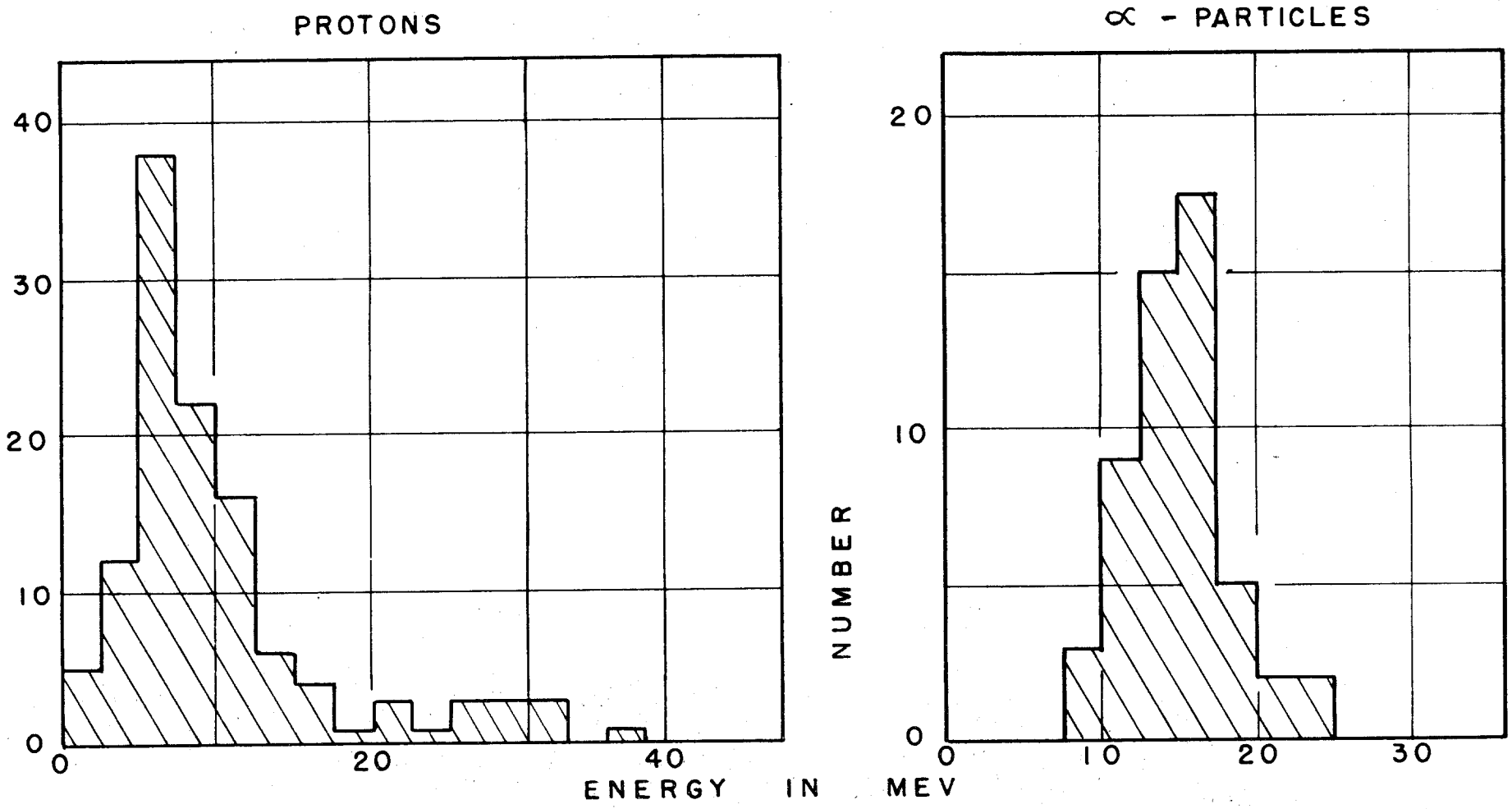

Figure 15. Energy distribution of protons and α-particles emitted from silver and bromine nuclei in stars with 3 to 6 black prongs. Observations with Ilford C2 emulsions.

Since most of the stars seen in photographic emulsions originate from silver or bromine, the preceding summary of nuclear stars refers mainly to the properties of stars arising from the disintegration of heavy nuclei. Experiments with sandwich emulsions indicate that multiply charged particles (mainly α-particles) account for about 50 percent of the tracks in stars originating from light elements.

The nuclear stars that are detected in the chamber are produced in the steel walls and in the argon gas. The assumption will be made that the general properties of these stars are the same as those of photographic emulsions.

The smallest pulses of the data that will be used, 5.7 volts, correspond to 18 times the average pulse produced by a singly charged minimum ionizing particle. Less than 1 percent of the total of stars produced in emulsions at $\lambda = 54^{\circ}$ and 94,000 feet have 18 or more shower particles (39 total prongs).[12] The effect of shower particles will therefore be neglected in calculating the effect of nuclear stars. Since there are from $2\frac{1}{2}$ to 3 times as many black tracks as grey tracks from a star, we will also neglect the effect of "grey" particles produced in the chamber wall and gas. "Grey" protons have a much longer range than "black" protons and thus a greater volume of material is effective in producing "grey" protons that can reach the chamber. Most of these "grey" protons will be produced in the atmosphere and will be considered under slow secondary protons, item (d).

In calculating the effect of nuclear stars, only the "black" particles will be considered, and the assumption made that there are five "black" particles with each star, three of which are protons and two of which are alpha particles. It will be assumed that the differential energy distribution of the "black" or evaporation particles is a constant from 10 to 20 Mev for α-particles and zero elsewhere, while for protons it will be assumed to be a constant from 4 to 12 Mev and zero elsewhere (see Figure 15). With the above simplifying assumptions, which, it is seen from the brief summary, are not too unreasonable, the effect of nuclear stars in the chamber will now be calculated.

Consider first the "black" protons. Let $G_P(R)\,dR$ be the differential range distribution of "black" protons produced per gram of material. This will be assumed to be the same for both steel and argon, a fact which is accurate enough for this calculation. Define $f(R)\,dR\,dS\,d\Omega$ as the number of "black" protons per second passing through an area dS of the chamber wall into the argon within the range interval $R \rightarrow R + dR$ and the solid angle $d\Omega$. Because the chamber wall is so much thinner than its diameter, in calculating $f_P(R)$ from $G_P(R)$ it can be assumed that the chamber wall is a plane. We thus see that

$$f_P(R)\,dR\,dS\,d\Omega = dR\,dS\,d\Omega \frac{\cos\theta}{4\pi} \int_0^{t/\cos\theta} G_P(x+R)\,dx. \quad (8)$$

$$G_P(R)\, dR = \frac{n}{\lambda}\, g_P(R)\, dR \ , \tag{9}$$

where $g_P(R)$ is the differential range distribution for each star,

n = total number of star-producing particles/cm^2-sec. in all directions (to be determined later),

λ = mean free path for producing stars.

It is assumed, as stated before, that the differential energy distribution of "black" protons per star is

$$\begin{aligned} n_P(E)\, dE &= 3/8\, dE \qquad && 4 \text{ Mev} \leq E \leq 12 \text{ Mev} \\ n_P(E)\, dE &= 0 \qquad && \text{otherwise.} \end{aligned} \tag{10}$$

Using the relationship

$$E = \left(\frac{R}{4.7}\right)^{.61} \ , \tag{11}$$

which holds very closely in steel when E is in Mev and R in milligrams/cm^2, we see that

$$g_P(R)\, dR = n_P(E)\, \frac{dE}{dR}\, dR = \frac{.089}{R^{.39}} \ . \tag{12}$$

Then

$$f_P(R) = \frac{3}{32}\, \frac{n \cos\theta}{\pi \lambda} \left[12 - \left(\frac{R}{4.7}\right)^{.61}\right] \ ,$$

$$47 \text{ mg/cm}^2 \leq R \leq 290 \text{ mg/cm}^2$$

$$f_P(R) = \frac{3}{4}\, \frac{n \cos\theta}{\pi \lambda} \qquad 0 \leq R \leq 47 \text{ mg/cm}^2 \tag{13}$$

In calculating $f_p(R)$, the fact was used that the range of the highest energy "black" protons, 290 mg/cm^2 of steel, was less than the thickness of the chamber wall, 465 mg/cm^2.

Introduce $H_p(E)\, dE\, dS\, d\Omega$ as the number of "black" protons per second passing through an area dS of the chamber wall into the argon within the energy interval $E \rightarrow E + dE$ and the solid angle $d\Omega$.

$$H_p(E) = f_p(R) \frac{dR}{dE} , \qquad (14)$$

$$H_p(E) = .72 \frac{n \cos\theta}{\pi\lambda} \left[12-E\right] E^{.64} , \qquad 4 \text{ Mev} \leq E \leq 12 \text{ Mev} ,$$

$$H_p(E) = 5.8 \frac{n \cos\theta}{\pi\lambda} E^{.64}, \qquad 0 \leq E \leq 4 \text{ Mev}. \qquad (15)$$

The total number of "black" protons per second going into the gas from the wall is

$$K_W^P = \iiint H(E)\, dE\, d\Omega\, dS = \frac{120\, n\pi D^2}{\lambda} , \qquad (16)$$

where D is the diameter of the sphere = 25.5 cm. K_W^P is not the number of pulses per second detected in the sphere from stars produced in the wall, because some stars will eject more than one "black" proton into the gas. To determine the number of pulses per second detected in the sphere because of stars produced in the wall, we will determine the average number of "black protons" per pulse detected in the gas.

Let A be the fraction of the total solid angle of 4π

such that a "black" proton ejected into A will reach the gas. Also define P_i as the probability that i black protons will reach the gas (i = 1, 2, 3).

$$P_1 = 3(1-A)^2 A.$$

$$P_2 = 3(1-A)A^2.$$

$$P_3 = A^3.$$

The average number of particles detected when a star is produced in the wall is

$$\bar{n} = \sum_{\ell=1}^{3} \ell P_\ell = 3A.$$

Let N(t) dt be the number of stars produced at depths between t and t + dt in the sphere wall.

N(t) dt = k dt where k is a constant and assuming the thickness of the wall is much smaller than the diameter of the sphere.

For simplicity we will assume that the range of all three protons from a star is the same and equal to R_P. The number of stars produced in the sphere wall with A in the interval dA is $N(A)\,dA = N(t)\,\frac{dt}{dA}\,dA = 2R_P k\,dA$, since $A = \frac{1 - \frac{t}{R_P}}{2}$.

Now the probability of detection of a star is $1 - (1 - A)^3$, so that the average number of prongs entering the gas per de-

tected star is

$$\frac{\int_0^{\frac{1}{2}} 3A\, n(A)\, dA}{\int_0^{\frac{1}{2}} \left[1-(1-A)^3\right] n(A)\, dA} = 1\,\frac{7}{17} \qquad (17)$$

Thus the number of pulses due to stars produced in the wall is

$$S_W^{(P)} = \frac{K_W^P}{1\ 7/17} = \frac{85 n \pi D^2}{\lambda} \qquad (18)$$

The number of stars per second produced in the gas of Chamber No. 14 is

$$S_G^{(P)} = \frac{4}{3}\pi\left(\frac{D}{2}\right)^2 \frac{n}{\lambda}\ \frac{145}{2} = 24.2\ \frac{\pi D^2 n}{\lambda}\ , \qquad (19)$$

where 145 is the equivalent milligrams/cm^2 of argon in the full pressure Chamber No. 14 for a diametrical transversal.

The ratio of the number of bursts produced by "black" protons from the wall and "black" protons from the gas is for Chamber No. 14

$$\frac{S_W^{(P)}}{S_G^P} = \frac{85}{24.2} = 3.5 \ .$$

It is thus seen that the wall is more important than the gas in producing black proton bursts in Chamber No. 14, and all the more so for Chamber No. 13, which has only 1/2.14 the mass of argon of No. 14. In addition, the stars produced in

the gas emit 2 "black" α-particles which will produce on the average many more ion pairs than the "black" protons from these stars, and we therefore can assume that the pulse size from these stars is determined by the "black" α-particles alone. For these reasons we can say that pulses produced by "black protons" are produced entirely by the wall.

By going through a completely analogous analysis of the pulses due to "black" α-particles, we find that the total number of "black" α-particles emitted into the gas,

$$K_W^{\alpha} = \frac{2 l n \pi D^2}{\lambda} , \tag{20}$$

and that the number of pulses due to "black" α-particles from the wall,

$$S_W^{\alpha} = 17.3 \frac{\pi n D^2}{\lambda} . \tag{21}$$

The number of pulses due to "black" α-particles produced in the argon gas of No. 14 is

$$S_{G14} = 22 \frac{n \pi D^2}{\lambda} , \tag{22}$$

and for No. 13 is

$$S_{G13} = 10 \frac{n \pi D^2}{\lambda} . \tag{23}$$

It is thus seen that the gas and wall are of about the same importance for the production of pulses due to "black" α-particles. It should be noted that some of the pulses classified as due to "black" α-particles and due to "black" protons may be the same pulse since it is possible that a "black" proton and α-particle from the same star may reach the gas. All stars produced in the gas emit both α's and protons, but since the pulses due to the α's are much larger than these due to protons, we will classify all pulses due to stars in the gas as "black" α-produced pulses.

We will next try to calculate how many of the pulses produced from stars in the wall emit both "black" α-particles and protons. To simplify the problem we will assume all "black" α-particles have the same range R_α and all "black" protons have the same range R_p. We take R_α equal to 43 mg/cm^2, the mean range of the assumed α-particle energy distribution. In the same way we take $R_p = 170$ mg/cm^2.

Consider the stars produced in the wall a distance t from the inner chamber surface ($R_\alpha \geq t \geq 0$). The probability of these stars emitting a proton into the argon is $1-(1-A_p)^3$, where A_p is the fraction of the solid angle where a proton passing into it reaches the gas. Likewise, for the α-particles the same probability is $1-(1-A_\alpha)^2$.

$$A_P = \frac{1 - \frac{t}{R_P}}{2} \quad .$$

$$A_\alpha = \frac{1 - \frac{t}{R_\alpha}}{2} \quad .$$

The probability of both an α and a proton being emitted into the gas is

$$P_{\alpha P} = [1-(1-A_P)^3][1-(1-A_\alpha)^2] \quad .$$

The number of stars between t and t + dt which emit both α's and protons into the gas is

$$dn_{\alpha P} = \frac{n\pi D^2}{\lambda} \, dt \, [1-(1-A_P)^3][1-(1-A_\alpha)^2]$$

$$n_{\alpha P} = \frac{n\pi D^2}{\lambda} \int_0^{R_\alpha} dt \, [1-(1-A_P)^3][1-(1-A_\alpha)^2] = \frac{15n\pi D^2}{\lambda} \quad , (24)$$

or about all of the "black" α pulses have also "black" protons, i.e., $n_{\alpha P} \approx S_W^\alpha$.

In order to correct for this overlap of "black" proton and "black" α-particle pulses, we will subtract $n_{\alpha P} \approx S_W^\alpha$ from $S_W^{(P)}$ and call the remainder S_W^P, the corrected number of "black" proton pulses from the wall. In other words, when a star ejects both "black" α-particles and protons into the gas, we are saying that the α-particles give the greatest contribution

to the pulse and we are calling that a "black" α pulse.

In summary, then,

$$S_W^P = S_W^{(P)} - S_W^{\alpha} = \frac{68n\pi D^2}{\lambda} \quad , \tag{25}$$

$$S_W^{\alpha} = \frac{17n\pi D^2}{\lambda} \quad , \tag{21}$$

$$S_{G13}^{\alpha} = \frac{10n\pi D^2}{\lambda} \quad , \tag{23}$$

$$S_{G14}^{\alpha} = \frac{22n\pi D^2}{\lambda} \quad . \tag{22}$$

In addition to the total number of pulses induced in the chambers by nuclear stars, it is necessary to know the differential or integral pulse size distribution. To do an exact calculation is very tedious and complicated, though straightforward enough. There is probably enough uncertainty in trying to determine the differential energy distribution of star particles in iron and argon from the data of photographic plates (which are mostly for bromine and silver), to make it meaningless to make an exact calculation. In addition this experiment was designed to try to determine experimentally the distribution of star pulses. For these reasons it is felt that the following approximate method is sufficient for the present purpose.

First, consider the "black" protons emitted from the wall. Any proton that stops in the chamber will give a pulse pro-

portional to its energy when emitted from the wall (neglecting potential effect) and independent of the pressure. Using Equation 13 , which gives the differential range distribution of "black" protons emitted from the wall, the number of protons that stop in Chamber No. 13 is

$$N_{13}^{P} = \pi D^2 \int_{\cos\theta=1}^{0} \int_{R=0}^{\ell} 2\pi f(R)\, dR\, d(\cos\theta),$$

where the symbols are defined in Figure 16. Using $\cos\theta = \frac{\ell}{D}$ we obtain

$$N_{13}^{P} = \pi D^2 \int_{\ell=0}^{D} \int_{R=0}^{\ell} \frac{2\pi}{D} f(R)\, dR\, d\ell = 36\, \frac{n\pi D^2}{\lambda} \quad . \tag{25}$$

In the same way, the number of protons that stop in Chamber No. 14 is

$$N_{14}^{P} = 64\, \frac{n\pi D^2}{\lambda} \quad . \tag{26}$$

Doing the analogous calculation for the "black" α-particles emitted from the wall, we obtain

$$N_{13}^{\alpha} = 17\, \frac{n\pi D^2}{\lambda} \quad , \tag{27}$$

$$N_{14}^{\alpha} = 20\, \frac{n\pi D^2}{\lambda} \quad . \tag{28}$$

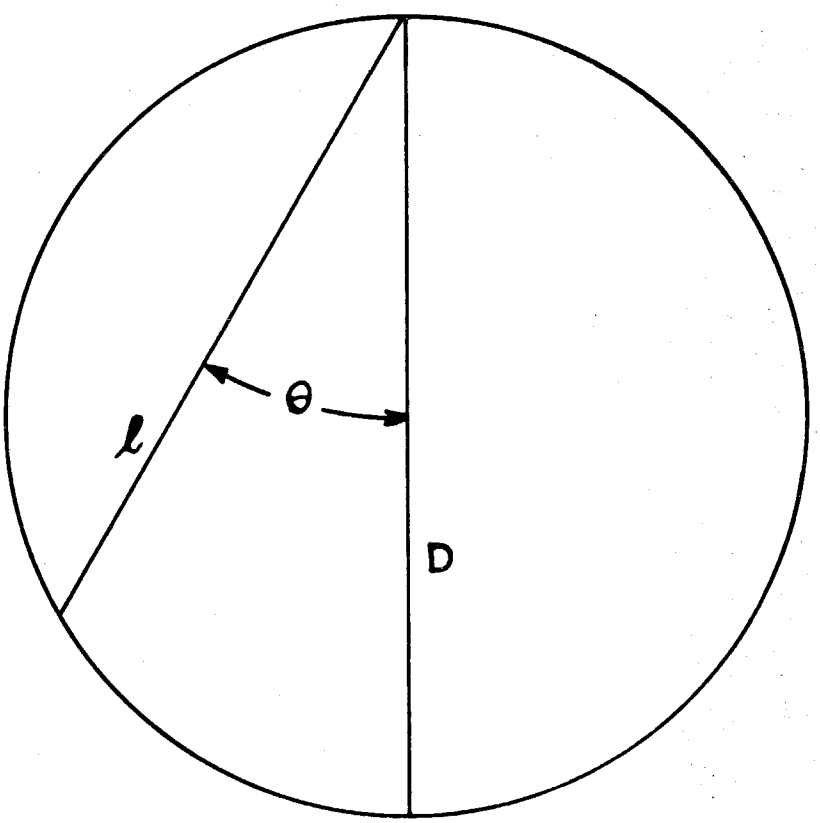

Figure 16. Diagram explaining the meaning of the symbols involved in calculating the number of star particles stopping in the spherical chambers.

The total number of "black" α-particles emitted from the wall is, from Equation 20,

$$K_w^{\alpha} = 21 \frac{n\pi D^2}{\lambda} \quad .$$

The number of pulses per second caused by these particles that stop in the chamber is, for Chambers No. 13 and No. 14,

$$S_{w13}^{P} = \frac{N_{13}^{P}}{1\frac{7}{17}} = \frac{26n\pi D^2}{\lambda} \quad , \tag{29}$$

$$S_{w14}^{P} = \frac{N_{14}^{P}}{1\frac{7}{17}} = \frac{45n\pi D^2}{\lambda} \quad , \tag{30}$$

$$S_{w13}^{\alpha} = \frac{N_{14}^{\alpha}}{1\frac{1}{5}} \quad \frac{14n\pi D^2}{\lambda} \quad , \tag{31}$$

$$S_{w14}^{\alpha} = \frac{N_{13}^{\alpha}}{1\frac{1}{5}} = \frac{17n\pi D^2}{\lambda} \quad . \tag{32}$$

The remaining star pulses which are due to particles that pass through both chambers are

$$S_{wthru}^{P} = S_{w}^{P} - S_{w14}^{P} = \frac{23n\pi D^2}{\lambda} \quad , \tag{33}$$

$$S^{\alpha}_{w\ thru} \approx 0 \quad . \tag{34}$$

We have just finished considering star particles originating in the wall only. To complete the picture we will consider those star particles originating in the gas. As was mentioned before, we only have to consider the α-particles ejected from the stars. We first calculate a quantity $f(\ell)$, which we define as follows. Consider the situation where there is a uniform production per unit volume of particles of range greater than the largest dimension of the chamber, all produced to move in the same direction and one particle per second is produced in the chamber. $f(\ell)\ d\ell$ is the number per second of particles that traverse a length $\ell \rightarrow \ell + d\ell$ before they escape. By referring to Figure 17 it is seen that

$$f(\ell)\ d\ell = \frac{\pi\left[\left(\frac{D}{2}\right)^2 - \left(\frac{\ell}{2}\right)^2\right] d\ell}{\frac{\pi D^3}{6}}$$

$$= \frac{3}{2D}\left(1 - \left(\frac{\ell}{D}\right)^2\right) d\ell \quad . \tag{35}$$

In Equation 35 the term $\frac{\pi D^3}{6}$ is the volume of the sphere and

$$\pi\ d\ell\left[\left(\frac{D}{2}\right)^2 - \left(\frac{\ell}{2}\right)^2\right]$$

is the volume of the region in Figure 17 between ℓ and $\ell + d\ell$.

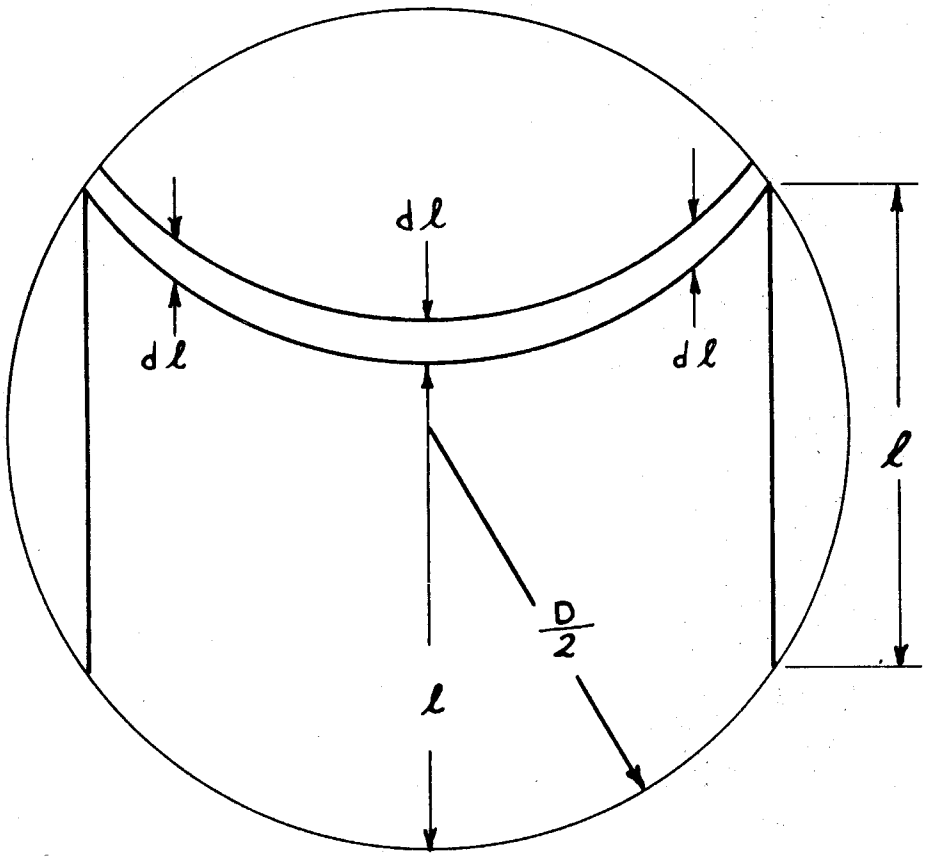

Figure 17. Diagram illustrating the calculation of $f(\ell)$.

Now consider that particles of range $R \leq D$ are produced uniformly in the chamber gas at the rate of n per second. The fraction of these that stops in the chamber is

$$\eta(R) = \frac{n\int_R^D f(\ell)\, d\ell}{n} = \frac{3}{2}\left[\frac{2}{3} - \frac{R}{D} + \frac{1}{3}\left(\frac{R}{D}\right)^3\right] \tag{36}$$

Let us now consider a uniform production of particles in the gas with a range distribution F(R) where F(R) dR is the number of particles produced per second with a range between R and R + dR.

N_D, the total number of particles that stop in the chamber per second, equals

$$\int_{R_{min}}^{R_{max}} F(R)\ \eta(R)\, dR \qquad (R_{max} \leq D). \tag{37}$$

In the chambers,

$$F(R) = \frac{1}{6}\pi D^2 \frac{nD'}{\lambda}\ g_\alpha(R) \tag{38}$$

where D = 25.5 cm, and D' = 68 mg/cm^2 for Chamber No. 13 and 145 mg/cm^2 for Chamber No. 14. From our assumed energy distribution of the "black" α-particles from a star and the range-energy relation for α-particles of $R = .57\ E^{1.57}$, where R is measured in mg/cm^2 and E in Mev, we obtain

$$g_{\alpha}(R) = \frac{.183}{R^{.36}} \qquad 21.5 \text{ mg/cm}^2 \leq R \leq 64 \text{ mg/cm}^2$$

$$g_{\alpha}(R) = 0 \qquad \text{otherwise} \quad . \tag{39}$$

Integrating Equation 37, using Equations 38 and 39, we obtain for the total number of particles that were produced in the gas and stop in the chamber,

$$N_D^{13} = 4.6 \frac{\pi D^2 n}{\lambda} \quad , \tag{40}$$

$$N_D^{14} = 27.1 \frac{\pi D^2 n}{\lambda} \quad . \tag{41}$$

The total number of particles produced in the chamber gas is

$$N_T = \int_{R_{min}}^{R_{max}} F(R)\, dR = \frac{1}{6} \pi D^2 \frac{nD'}{\lambda} \int_{21.5}^{64} \frac{.183\, dR}{R^{.36}}$$

$$N_T^{13} = 23 \frac{\pi D^2 n}{\lambda} \tag{42}$$

$$N_T^{14} = 49 \frac{\pi D^2 n}{\lambda} \tag{43}$$

As a check we note that Equation 43 should equal twice Equation 19, since two particles are produced per star, which it does.

The fraction of particles that stop in the chambers is from Equations 40-43.

$$\epsilon_{13} = \frac{4.6}{23} = .20 \qquad (44)$$

$$\epsilon_{14} = \frac{27.1}{49} = .55 \qquad (45)$$

We are assuming that two α-particles are emitted from each star. The largest contribution to the pulse from the star will come almost always from the particle or particles, if any, that stop in the chamber. We will try to estimate how many pulses are caused by at least one particle stopping in the chamber. For Chamber No. 13 the average probability that a particle does not stop in the chamber is 1 - .20 = .80. The probability that both particles from a star do not stop in the chamber is $.80^2 = .64$, or the probability that at least one particle stops in the chamber is $P_S^{13} = 1 - .64 = .36$. In the same way $P_S^{14} = 1 - .45^2 = .80$.

The total number of pulses caused by at least one particle stopping in the chamber is

$$S_{G14}^{\alpha} = \tfrac{1}{2} P_S^{14} N_T^{14} = 19.5 \frac{\pi D^2 n}{\lambda} , \qquad (46)$$

$$S_{G13}^{\alpha} = \tfrac{1}{2} P_S^{13} N_T^{13} = 4.2 \frac{\pi D^2 n}{\lambda} . \qquad (47)$$

The factor of $\frac{1}{2}$ in Equations 46 and 47 is used because there are two particles for each star.

As was stated before, any pulse caused by particles stopping in the chamber gas is dependent only on the energy of the particle and independent of the gas pressure. Let us denote the integral pulse height distribution due to all such pulses as $B^i(S)$, where i = 13 or 14 depending on the chamber in question, and S is the pulse size in volts. We have in our preceding analysis divided $B^i(S)$ into two classes, one class consisting of all of the pulses produced by "black" α-particles coming from the wall and the gas and stopping in the chamber gas, and the other class consisting of pulses produced by "black" protons originating in the wall and stopping in the chamber gas. In general the "black" proton pulses will be smaller than the "black" α pulses. The largest pulse that can be produced by a single particle is by one that stops just after traversing the path length in the chamber giving the maximum pulse. (This path has a minimum distance from the center of the sphere of 2.24 inches (See Equation 6a)). For Sphere No. 14 these maximum pulses for protons and α-particles are 1.15 Po-α pulse and 4.57 Po-α pulse, respectively. For Sphere No. 13 these maximum pulses are .77 Po-α pulse and 2.86 Po-α pulse for protons and for α-particles, respectively.

We now calculate $B^i(0)$, the total number of pulses caused by at least one particle stopping in the gas. From

Equations 47, 29, and 31,

$$B^{13}(0) = S^{\alpha}_{G13} + S^{P}_{w13} + S^{\alpha}_{w13} = 44\ \frac{n\pi D^2}{\lambda} \quad . \tag{48}$$

From Equations 46, 30, and 32,

$$B^{14}(0) = S^{\alpha}_{G14} + S^{P}_{w14} + S^{\alpha}_{w14} = 81\ \frac{n\pi D^2}{\lambda} \quad . \tag{49}$$

$$\frac{B^{14}(0)}{B^{13}(0)} = 1.84 \tag{50}$$

The contribution to $B(0)$ by α-induced pulses (the larger pulses) is from Equations 47 and 31,

$$B^{13}_{\alpha} = S^{\alpha}_{G13} + S^{\alpha}_{w13} = 18\ \frac{n\pi D^2}{\lambda}, \tag{51}$$

and from Equations 46 and 32,

$$B^{14}_{\alpha} = S^{\alpha}_{G14} + S^{\alpha}_{w14} = 36\ \frac{n\pi D^2}{\lambda} \quad . \tag{52}$$

$$\frac{B^{14}_{\alpha}}{B^{13}_{\alpha}} = 2.0$$

It is now necessary to consider those star pulses where all the star particles pass through the chamber. Denote the integral pulse height distribution due to these particles by $\Delta^{i}(S)$, $i = 13, 14$.

From Equations 42, 47, 25, and 29,

$$\Delta^{13}(0) = \frac{N_T^{13}}{2} - S_{G13}^{\alpha} + S_w^P - S_{w13}^P = 49\,\frac{n\pi D^2}{\lambda} \quad . \tag{54}$$

From Equations 43, 46, 25, and 30,

$$\Delta^{14}(0) = \frac{N_T^{14}}{2} - S_{G14}^{\alpha} + S_w^P - S_{w14}^P = 28\,\frac{n\pi D^2}{\lambda} \quad . \tag{55}$$

The contribution of α-particle pulses to $\Delta(S)$ is

$$\Delta_{\alpha}^{13} = \frac{N_T^{13}}{2} - S_{G13}^{\alpha} = 7\,\frac{n\pi D^2}{\lambda} \quad , \tag{56}$$

and

$$\Delta_{\alpha}^{14} = \frac{N_T^{14}}{2} - S_{G14}^{\alpha} = 5\,\frac{n\pi D^2}{\lambda} \quad . \tag{57}$$

In summary, we find it convenient to divide the pulses due to nuclear interactions into two classes, one in which the pulses are caused by at least one particle stopping in the gas of the chamber, and the other consisting of all other pulses. Each of these classes is further divided into two subclasses, those pulses produced from α-particles and those produced from protons. The number in each class is summarized as follows.

For Chamber No. 13:

$$B^{13}(0) = 44 \frac{n\pi D^2}{\lambda} , \tag{48}$$

$$B_{\alpha}^{13} = 18 \frac{n\pi D^2}{\lambda} , \tag{51}$$

$$\Delta^{13}(0) = 49 \frac{n\pi D^2}{\lambda} , \tag{54}$$

$$\Delta_{\alpha}^{13} = 7 \frac{n\pi D^2}{\lambda} . \tag{56}$$

For Chamber No. 14:

$$B^{14}(0) = 81 \frac{n\pi D^2}{\lambda} , \tag{49}$$

$$B_{\alpha}^{14} = 36 \frac{n\pi D^2}{\lambda} , \tag{52}$$

$$\Delta^{14}(0) = 28 \frac{n\pi D^2}{\lambda} , \tag{55}$$

$$\Delta_{\alpha}^{14} = 5 \frac{n\pi D^2}{\lambda} . \tag{57}$$

Slow Secondary Protons

At the altitude where the flight data were taken, 15 g/cm^2, 45 percent of the primary protons will have interacted with air nuclei, assuming a geometric cross section of 68 g/cm^2, before reaching the chamber. It is thus import-

ant to consider the low energy secondaries from these interactions and to find their effect on the counting rate of the chamber. Geomagnetic cutoff energy for protons at $\lambda = 55^{o}$ is 1.14 Bev, corresponding to a range in the atmosphere of 440 g/cm^2. Protons incident horizontally at the top of the atmosphere will have to go through about 460 g/cm^2 of atmosphere before reaching the chamber. If no interactions with the air occur it is conceivable that some of the incident protons will lose sufficient energy by ionization losses to be able to ionize very heavily in the chamber and produce a detectable pulse. But since the collision mean free path in air is 68 g/cm^2 the primaries will interact before this will happen. It is thus necessary to consider only the secondary protons. Rossi [13] calculated the differential energy distribution of secondary protons moving in the vertical direction at 700 g/cm^2 atmospheric depth. Although this calculation is not exact and was not calculated for near the top of the atmosphere, it should give a sufficiently good estimate of the relative differential energy distribution at 15 g/cm^2 of the secondary protons only.

About 1000 protons per second pass through the sphere at 15 g/cm^2, which is of the order of magnitude of the secondary protons passing through the chamber. To give a pulse of 2 volts or more in Chamber No. 14, a particle must ionize at least 7 times minimum. From Reference (13) it is calculated that about 13 counts per second come from protons with energy less than or equal to 38 Mev. This is a large fraction of

the total counts at 2 volts. To give a 5.7 volt pulse the proton energy has to be less than or equal to 12 Mev. These protons contribute less than 1 count per second, which is a small fraction of the total counts at 5.7 volts. We will therefore not use the data in Figure 14 from 2 volts to 5.7 volts. We will assume that there is a negligible effect of slow secondary protons for pulses greater than 5.7 volts in Chamber No. 14.

Slow α-Particles

The effect of slow α-particles will be discussed under the section INTERPRETATION OF RESULTS.

Electron Showers

The simultaneous passage of 18 electrons through Chamber No. 14 is required to produce an average pulse of 5.7 volts. This corresponds to a shower density of 360 particles per square meter. At the pressure of 15 g/cm^2 it appears, from experimental results [14] and theoretical reasoning, that the number of showers of this density or greater is negligible. This result is in agreement with Coor.[9]

The chamber wall is only about 4 percent of a shower radiation length, so that the probability of producing in the wall a cascade shower with 18 or more electrons is negligible.

Pileup of Small Pulses

Singly charged ionizing particles are passing through the chamber at the rate of about 1000 counts per second. The average pulse, which is equal to 5/6 S_{max}^{min} (see Equation 7.1 and Figure 3) due to a singly charged minimum ionizing particle, is .31 volts in Chamber No. 14 (Table IV). The root mean square voltage produced by n particles per second, where each particle produces a time response voltage of f(t), is $\sigma = \sqrt{n \int_{-\infty}^{\infty} f(t)^2 \, dt}$.(15) At the output of the amplifier the pulse due to a singly ionizing particle is about .3 volt high and lasts for about 100 μsec. Under these conditions $\sigma \approx \sqrt{1000(.3^2 \times 10^{-4})} \approx .1$ volt. Thus the pileup of these pulses is negligible.

INTERPRETATION OF RESULTS

In the previous section it was shown that, except for slow α-particles which will be corrected for later, for pulses greater than 5.7 volts in Chamber No. 14 (which corresponds to 2.7 volts in Chamber No. 13), the only appreciable background is due to nuclear stars. It was also shown in the previous section that the pulses measured in the chamber can be divided into three groups. This can be summarized by the following equation:

$$M^i(S) = B^i(S) + \Delta^i(S) + C^i(S), \qquad i = 14, 13, \qquad (58)$$

where $M^i(S)$ is the integral pulse height distribution measured in the chamber i,

$B^i(S)$ is the integral pulse height distribution due to evaporation star particles stopping in the chamber i,

$\Delta^i(S)$ is the integral pulse height distribution due to evaporation star particles passing through the chamber i,

and $C^i(S)$ is the integral pulse height distribution due to cosmic-ray particles, primaries or secondaries, which pass through the chamber i.

It follows from the definition of the quantities that

$C^{13}(S) = C^{14}(2.14S) \equiv C(2.14S)$. From Equation 50 we see that for small pulses ($S \approx 0$) $B^{14}(S) = 1.84\ B^{13}(S)$, and from Equation 53, that for large pulses $B^{14}(S) = 2.0\ B^{13}(S)$. The assumption will be made that $B^{14}(S) = 2\ B^{13}(S)$ for all S. Using these relations we obtain from Equation 58,

$$M^{14}(S) = 2\ B^{13}(S) + C(S) + \Delta^{14}(S) \tag{59}$$

$$M^{13}(S) = B^{13}(S) + C(2.14S) + \Delta^{13}(S) \tag{60}$$

Introduce

$$g(S) \equiv M^{13}(S) - M^{14}(2.14S) \tag{61}$$

$$g(S) = B^{13}(S) - 2B^{13}(2.14S) + \Delta^{13}(S) - \Delta^{14}(2.14S) \tag{62}$$

Since the smallest value of S to be taken is 5.7 volts, 2.14 S has a smallest value of 12.2 volts or .94 Po-α pulse. Only protons between 7.5 Mev and 8.7 Mev can give that size of a pulse in Chamber No. 14 and still pass through the chamber, and then only for certain limited paths through the chamber. In other words, most of the pulses of $\Delta^{13}(S)$ are smaller than 5.7 volts and most of those of $\Delta^{14}(S)$ are smaller than 12.2 volts. We will therefore neglect $\Delta^{i}(S)$. Then

$$g(S) = B^{13}(S) - 2B^{13}(2.14S) \quad , \text{ and}$$

$$B^{13}(S) = g(S) + 2B^{13}(2.14S) \quad . \tag{63}$$

$$B^{13}(S) = \sum_{n=0}^{\infty} 2^n \, g(2.14^n S) \tag{64}$$

$$B^{14}(S) = 2B^{13}(S) = \sum_{n=0}^{\infty} 2^{n+1} \, g(2.14^n S) \tag{65}$$

The result of this calculation using the data in Figures 13 and 14 is shown in Figure 18. From Equation 49, we see that

$$B^{14}(0) = \frac{81n\pi D^2}{\lambda} \quad .$$

The geometric mean free path in iron, λ , is 106×10^3 mg/cm^2. Evidence from photographic plates [12] indicates that at the latitude and altitude of the balloon flight of this experiment about one-half of the stars is produced by uncharged particles and about one-half is produced by charged particles. The total number of charged particles passing through a sphere of unit cross section at the flight altitude is about 1.5 per second. n is therefore twice this value or about 3 per second.

$$B^{14}(0) \approx \frac{81 \times 3\pi \times (25.5)^2}{10^5} \approx 5 \text{ per second.}$$

It is seen that the experimental results of Figure 18 are consistent with this theoretical value.

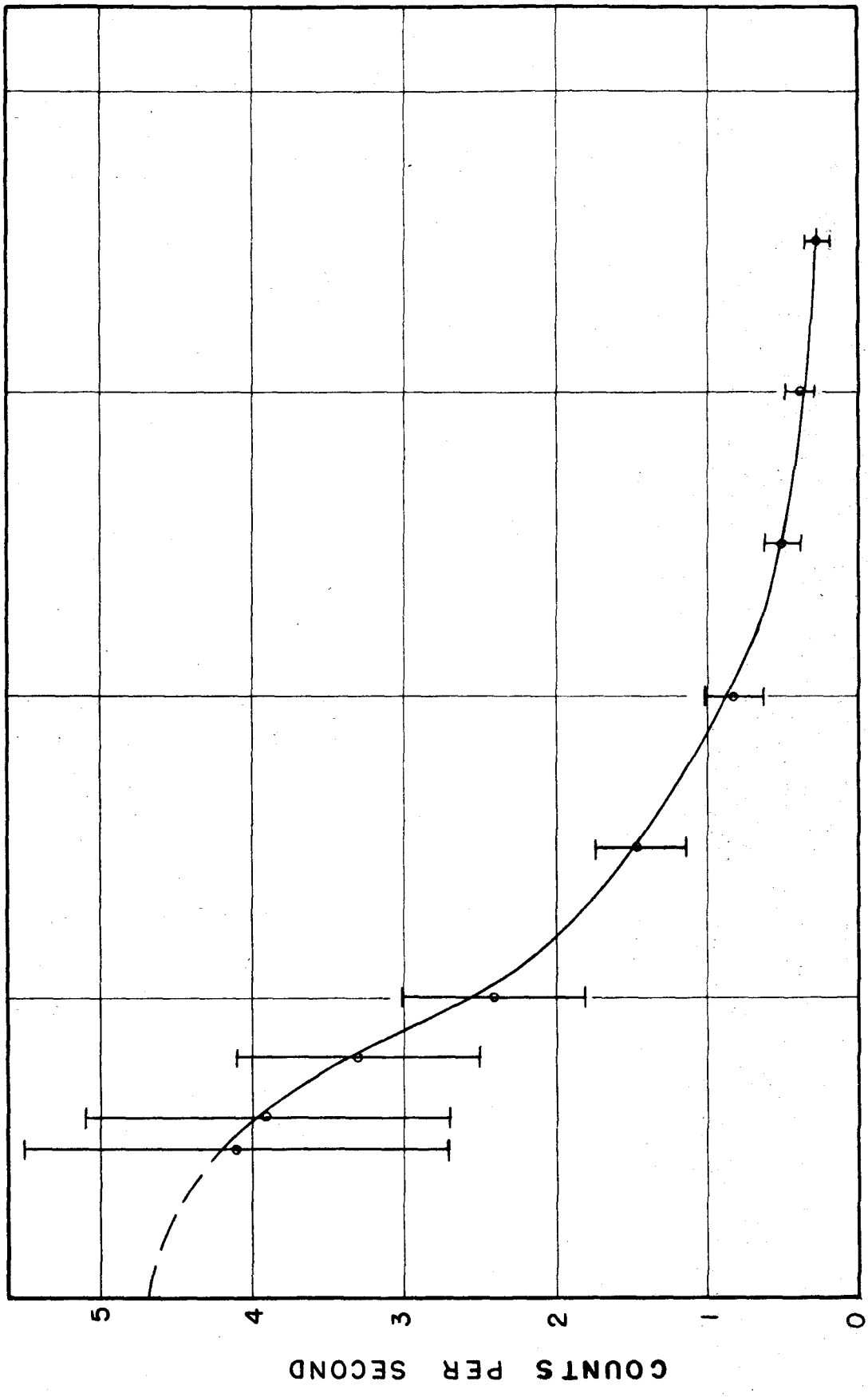

Figure 17. The experimentally determined integral pulse height distribution, $E^{14}(S)$, produced in Chamber No. 14 by star particles that stop in the chamber. The errors shown are statistical and an estimate of uncertainties caused by errors in the measurement of pulse sizes.

Because g(S) is the difference (Equation 62) between the counting rates of the two chambers, it, and therefore B(S), is very sensitive to any errors. The ratio of the gas pressures in the two chambers is known to within 1 percent, and the ratio of the pulses due to Po α-particles is known to within about 4 percent (see Table III). There is also a small indeterminacy of a few tenths of a volt in the small pulse sizes, due to uncertainty in the grid current correction and in the measurement of the beginning bias voltage. These errors can be more important than the statistical errors. The errors indicated in Figure 18 are an estimate of these errors and the statistical errors.

The ionization of a particle varies as $Z^2 f(\beta)$. If all particles passing through the chamber were relativistic, the ionization would uniquely determine the charge. At $\lambda = 55^\circ$ the minimum allowed energy at the vertical is .3 Bev per nucleon. Thus it is seen that the particles are not all relativistic. It is necessary to account for this. From photographic emulsion work it is shown[16] that the differential energy spectrum for all heavy particles $Z \geq 2$ is of the form

$$N(\varepsilon)\, d\varepsilon = \frac{A_Z}{(1+\varepsilon)^{2.35}}\, d\varepsilon$$

where A_Z is a constant depending on Z and ε is the energy per nucleon measured in Bev. A calculation shows that the pulse

distribution in the chamber at $\lambda = 55^{\circ}$ is not too sensitive to the assumed energy distribution of the incident particles.

Assuming an isotropic incidence on the top of the atmosphere of particles of charge Z whose differential energy distribution per second and unit area is

$$2\pi \sin\theta \, \eta_Z(\varepsilon,\theta,0) \, d\varepsilon \, d\theta = \frac{2\pi \sin\theta \, K_Z}{(1+\varepsilon)^{2.35}} \, d\varepsilon \, d\theta \qquad (66)$$

we will determine the energy distribution at the chamber, taking into account ionization loss and collision loss. K_Z is a constant and θ is the angle to the vertical.

At a distance h g/cm^2 below the top of the atmosphere the new distribution in the direction θ is

$$\eta_Z(\varepsilon',\theta,X) = \eta_Z(\varepsilon,\theta,0) \, \frac{\partial(\varepsilon,\theta)}{\partial(\varepsilon',\theta)} \, , \quad \left(X = \frac{h}{\cos\theta}\right) \qquad (67)$$

where $\frac{\partial(\varepsilon,\theta)}{\partial(\varepsilon',\theta)}$ is the Jacobian of the transformation and is equal to

$$\left(\begin{vmatrix} \frac{\partial\varepsilon'}{\partial\varepsilon} & \frac{\partial\varepsilon'}{\partial\theta} \\ \frac{\partial\theta}{\partial\varepsilon} & \frac{\partial\theta}{\partial\theta} \end{vmatrix} \right)^{-1} = \frac{1}{\frac{d\varepsilon'}{d\varepsilon}} \, . \qquad (68)$$

For non-relativistic particles the following relationship exists in air:

$$\varepsilon = C_Z R^{.56} \tag{69}$$

where R is the range of the particle and C_Z is a constant depending on Z.

The change in the shape of the differential energy curve due to ionization loss is only important for non-relativistic particles where the given relationship is valid, and though the relationship is not valid for relativistic particles the ratio $\frac{d\varepsilon'}{d\varepsilon}$ is very closely correct for such particles. It is therefore sufficiently accurate to use the relationship $\varepsilon = C_Z R^{.56}$ for all energies.

Using Equations 67, 68, and 69, we see that

$$n_Z(\varepsilon', \theta, X) = \left(\frac{R_o - X}{R_o}\right)^{.44} \frac{K_Z e^{-\frac{x}{\lambda_Z}}}{\left(1 + C_Z R_o^{.56}\right)^{2.35}} \tag{70}$$

$R_o = \left(\frac{\varepsilon'}{C_Z}\right)^{\frac{1}{.56}} + X$ and λ_Z is the mean free path for collisions, assumed to be independent of energy. The smallest value of R_o is determined by the cutoff and at 55^o is equal to $\left(\frac{.3}{C_Z}\right)^{\frac{1}{.56}}$.

To find the distribution in pulses per second at the chamber we must integrate over all angles and over the cross section.

$$N_Z(\varepsilon', h) = \frac{\pi D^2}{4} \int_0^{\pi/2} 2\pi \sin\theta \; n_Z(\varepsilon', \theta, X) \; d\theta$$

$$= \frac{\pi^2 D^2}{2} \int_0^{\pi/2} \sin\theta \; \frac{A^{.44}}{(A+X)^{.44}} \; \frac{K_Z e^{-\frac{X}{\lambda_Z}}}{\left(1+C_Z(A+X)^{.56}\right)^{2.35}} \, d\theta \,, \tag{71}$$

where $A = R_o - X$ is constant during the integration.

This integration was performed numerically for several different Z's, and it was found that for all $Z \geq 3$ there was not a significant difference in the shape of $N_Z(\varepsilon', h)$. In this calculation the following values were used, R being measured in mg/cm^2:

C_2	= .030	λ_2	= 45 gm/cm^2 of air.
C_5	= .050	λ_5	= 30 gm/cm^2
C_8	= .065	λ_8	= 25 gm/cm^2
C_{14}	= .089	λ_{14}	= 18 gm/cm^2
C_{20}	= .109	λ_{20}	= 18 gm/cm^2

By combining the energy distribution at the chamber, $N_Z(\varepsilon', 15)$, and the integral pulse height distribution with fluctuations (shown in Figure 4) calculated for minimum ionizing particles, we obtain the theoretical integral pulse

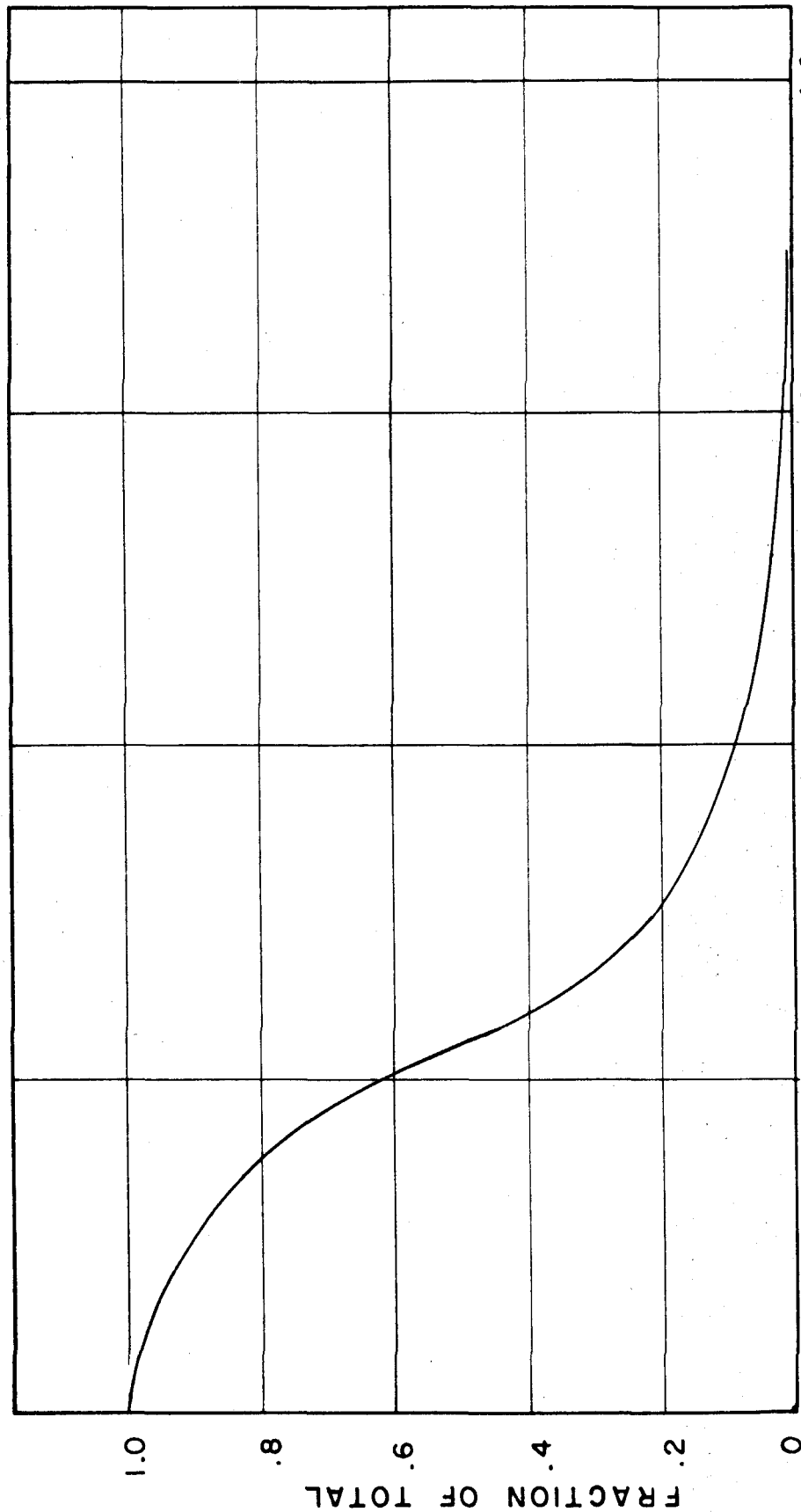

Figure 19. Theoretical integral pulse height curve for α-particles considering 3 volt amplifier noise, the energy distribution of α-particles at the sphere, and statistical fluctuations in energy loss.

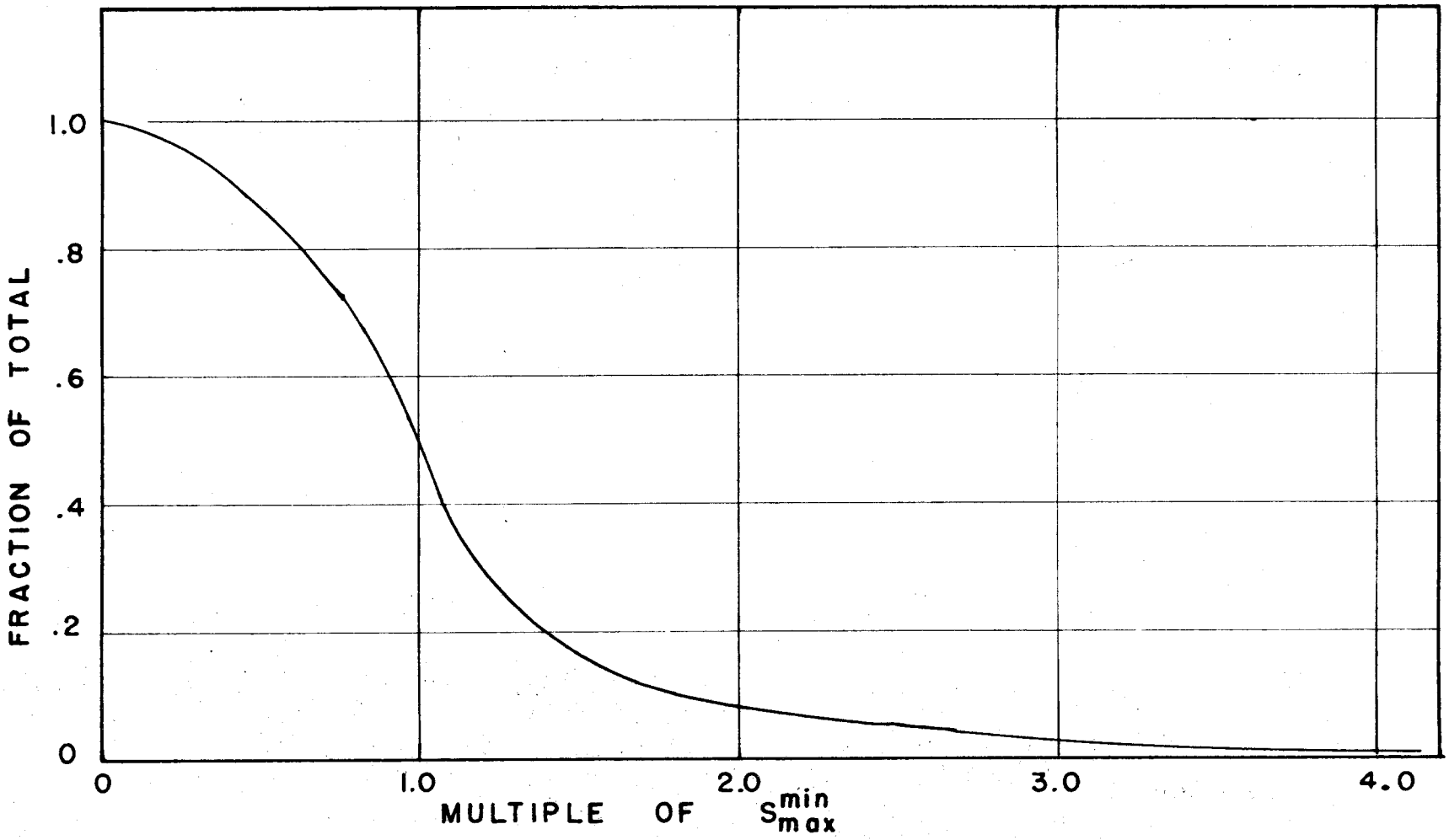

Figure 20. Theoretical integral pulse height curve for particles $2 < Z < 20$. This calculation considers the energy distribution of the heavy particles at the chamber and statistical fluctuations in energy loss.

height distributions for $Z = 2$ and $Z \geq 3$ shown in Figures 19 and 20.

The promised correction for slow α-particles can now be made from the information contained in Figure 19. This correction includes only those primary α-particles that have slowed down due to ionization loss. Slow α-particles are also produced in nuclear stars and in the fragmentation of heavier nuclei. The slow α-particles from nuclear stars have been accounted for already under nuclear stars. The heavier nuclei are less numerous than α-particles in the primary flux, but about 2 α-particles are produced in each collision of a heavy nucleus ($Z \geq 10$), and about 1.5 α-particles in each collision of a medium nucleus ($6 \leq Z \leq 10$), with an air nucleus.[17] The α-particles produced in the fragmentation of a heavy nucleus are, in the frame of reference of the heavy nuclei, evaporation α-particles. These particles have low energies with respect to that frame of reference, and in the laboratory system these α-particles will have practically the same velocity distribution as the incident heavy nuclei. These α-particles can be accounted for, to a good enough approximation, by merely adding about 15 percent to the primary α-particles values, because the velocity distribution for all particles $Z \geq 2$ is practically the same.

ANALYSIS OF DATA

The following procedure was used in analyzing the data. From the integral pulse height distributions of Figures 19 and 20 and Table IV, the fraction of the total number of each heavy particle contributing to the pulses at a given voltage in Chamber No. 14 was calculated. Thus, for example, the counting rate at 5.7 volts in Chamber No. 14 consists of

1	percent	of	the	total	number	of	α-particles,
11	"	"	"	"	"	"	Li particles,
50	"	"	"	"	"	"	Be "
80	"	"	"	"	"	"	B "
89	"	"	"	"	"	"	C "
93	"	"	"	"	"	"	N "
95	"	"	"	"	"	"	O "
96	"	"	"	"	"	"	F "
97	"	"	"	"	"	"	Ne "
$\approx$ 100	"	"	"	"	"	"	$Z > 10$ particles

and background counts consisting mostly of $B^{14}(5.7)$.

The difference in counting rate was next taken between various voltages in Figure 14. The contribution of $B^{14}(S)$ to this difference was found from Figure 18. The remaining counts consisted of known fractions of various Z particles. By this means it was possible to obtain the amounts of Be,

B, C, N, O, and heavier nuclei ($Z \geq 9$) passing through the chamber. The results are shown in Table V. Statistical errors and the uncertainty in the background correction, $B^{14}(S)$, are reflected in the large errors.

It is of interest to determine the composition of the counting rate at 28.6 volts = 2.2 Po-α pulse. The counting rate at this voltage is composed of the following percentages of the heavy nuclei:

Z	Percent	Counts/sec.
4	.8	$.07 \pm .035$
5	3	
6	7	$.37 \pm .13$
7	13	
8	27	
9	53	
10	71	
11	79	
12	84	
≥ 13	≈ 100	

From Figure 14, the counting rate at 28.6 volts = $1.05 \pm .023$. The star contribution (Figure 18) at 28.6 volts is $.39 \pm .05$. The contribution to the counting rate due to the long tail of the integral pulse height distribution of Be, B, C, N, and O is, from Table V, $.44 \pm .13$. The remaining counts, which are approximately due to $Z \geq 9$, are $.22 \pm .13$ counts per second.

Table V. Heavy particle flux at $\lambda = 55^{\circ}$.

Charge Group	Counts/sec. in Chamber #14	Flux Extrapolated to the Top of the Atm. (particles/m^2-steradian-sec.)	Other Observers	Lowest Effective ε^e for this Experiment
$Z = 4,5$	3.3 ± 1.9	22.5 ± 13 [b]	10 ± 1 [d]	.3 Bev
			5.3 ± 1.9 [c]	
$3 \leq Z \leq 5$				
$6 \leq Z \leq 8$ [a]	2.7 ± 1.0	24 ± 9 [b]		.4 Bev
$6 \leq Z \leq 9$ [a]			12 ± 1 [d]	
$6 \leq Z \leq 10$ [a]			11.5 ± 1.7 [c]	
$Z \geq 9$ [a]	$.25\pm.14$	2.9 ± 1.6 [b]		.7 Bev
$Z > 9$ [a]			$4.2\pm.6$ [d]	
$Z > 10$ [a]			3.0 ± 1.2 [c]	

a. The flux of the particles with $Z = 9$ and 10 is very small. The groups $6 \leq Z \leq 8$, $6 \leq Z \leq 9$, and $6 \leq Z \leq 10$ should have practically the same flux values. This is also true of the groups $Z \geq 9$, $Z > 9$, and $Z > 10$.
b. This experiment.
c. Reference 18.
d. Reference 19.
e. ε is measured in Bev per nucleon.

It should be noted that the tail of the integral pulse height curve produces more counts than any other single cause. If statistical fluctuations in the ionization loss were not considered, one would have said that no counts are due to Be, B, C, N, and O at 28.6 volts and would have then obtained more than twice the flux for $Z \geq 9$.

EXTRAPOLATION TO THE TOP OF THE ATMOSPHERE

In order to obtain the flux values of the heavy particles at the top of the atmosphere, it is necessary to extrapolate the values measured at the chamber back through the residual atmosphere taking into account interactions that occur. Because the heavy nuclei fragment into lighter heavy nuclei in collisions with the air, the attenuation through the atmosphere does not vary exponentially, but the diffusion equations must be solved. These equations are, for the direction θ, using the notation of Kaplon, Noon and Racette,[18] and neglecting ionization loss,

$$\frac{dN_I(X)}{dX} = -\frac{N_I(X)}{\lambda_I} + \sum_{I' \geq I} P_{I'I} \frac{N_{I'}(X)}{\lambda_{I'}} ,$$

where λ_I is the mean free path in g/cm^2 of atmosphere for the Ith component of the heavy element flux, $P_{I'I}$ is the probability that in an interaction of a nucleus of type I'

a nucleus of type I (of assumed comparable momentum per nucleon) is emitted, $X = \frac{h}{\cos\theta}$ is the amount of atmosphere traversed, h the vertical depth below the top of the atmosphere, and θ the zenith angle. In addition, the nuclei are classified into three charge groups: L nuclei ($4 \leq Z \leq 5$) with mean Z = 4.6 (notice that this is not the same as the usual definition where $3 \leq Z \leq 5$); M nuclei ($6 \leq Z \leq 8$) with mean Z = 7; and H nuclei ($Z \geq 9$) with mean Z = 15. The solutions to these equations are

$$N_H(X) = N_H^\circ e^{-\frac{X}{\lambda_H'}} ,$$

$$N_M(X) = N_M^\circ e^{-\frac{X}{\lambda_M'}} + \frac{\alpha_{HM} P_{HM}}{\lambda_H}\left(N_H^\circ e^{-\frac{X}{\lambda_M'}} - N_H(X)\right) ,$$

$$N_L(X) = N_L^\circ e^{-\frac{X}{\lambda_L'}} + \frac{\alpha_{ML} P_{ML}}{\lambda_M}\left(N_M^\circ e^{-\frac{X}{\lambda_L'}} - N_H(X)\right)$$

$$+ \frac{\alpha_{HL}}{\lambda_H}\left(P_{HL} + \frac{P_{HM} P_{ML} \alpha_{ML}}{\lambda_M}\right)\left(N_H^\circ e^{-\frac{X}{\lambda_L'}} - N_H(X)\right),$$

where $\lambda_I' = \frac{\lambda_I}{(1 - P_{II})}$, $\alpha_{IJ} = \frac{\lambda_I' \lambda_J'}{\lambda_J' - \lambda_I'} > 0$;

$\lambda_J' > \lambda_I'$, and N_I° is the incident flux of type I at the top of the atmosphere (assumed isotropic). In the above, the

first term on the right-hand side represents the absorption of the incident flux of type I, while the other terms represent the contribution to this flux by breakup of the heavier flux.

In this experiment the particles were measured in all directions, requiring the integration of $N_I(X)$ over the upper hemisphere of 2π. The only quantity of $N_I(X)$ that varies with angle is of the form $e^{-\frac{h}{\lambda_I' \cos\theta}}$. Integrating this over the upper hemisphere, we obtain

$$2\pi \int_0^1 e^{-\frac{h}{\lambda_I' \cos\theta}} d(\cos\theta)$$

Introduce $y = \frac{h}{\cos\theta}$. Then $d(\cos\theta) = -\frac{h}{y^2} dy$, and

$$\int_0^1 e^{-\frac{h}{\lambda_I' \cos\theta}} d(\cos\theta) = h \int_h^\infty \frac{e^{-\frac{y}{\lambda_I'}}}{y^2} dy$$

$$= h \left[\frac{e^{-\frac{h}{\lambda_I'}}}{h} - \frac{1}{\lambda_I'} \int_{\frac{h}{\lambda_I'}}^\infty \frac{e^{-u}}{u} du \right] .$$

Thus in order to convert the diffusion equations so as to be applicable for the spherical chamber it is only necessary to replace $e^{-\frac{h}{\lambda_I'}}$ by

$$A_{I'} \equiv \left[e^{-\frac{h}{\lambda_I'}} - \frac{h}{\lambda_I'} \int_{\frac{h}{\lambda_I'}}^\infty \frac{e^{-u}}{u} du \right]$$

The following values of the parameters were used:[18] $\lambda_L = 31.5$ g/cm^2, $\lambda_M = 26.5$ g/cm^2, $\lambda_H = 18$ g/cm^2, $P_{LL} = .07$, $P_{MM} = .13$, $P_{HH} = .25$, $P_{HM} = .27$, $P_{ML} = .21$, and $P_{HL} = .24$. The values used for P_{HL}, P_{ML}, and P_{LL} are one-half those given by Reference 18. This is necessary because the definition used here for the L nuclei differs from that of Reference 18 in that Li is not included. Experimental results [17] indicate that Li composes about one-half of all the Li, Be, and B fragments of the heavier nuclei.

Introducing into the solutions of the diffusion equations for the spherical chamber the above values of the parameters, we obtain at $h = 15$ g/cm^2,

$$N_H(X) = .266\, N_H^{\circ} \tag{72a}$$

$$N_M(X) = .332\, N_M^{\circ} + .425\, N_H(X) \tag{72b}$$

$$N_L(X) = .361\, N_L^{\circ} + .207\, N_M(X) + .450\, N_H(X) \tag{72c}$$

It is of interest to note that these equations show that the heavy particles, when measured at 15 g/cm^2 with spherical geometry so that particles from all directions are detected, are attenuated the same amount that a vertical detector would measure at 32 g/cm^2.

The geometric factor to convert the intensity in a spherical chamber to intensity per unit area and solid angle

is 2 π^2 r^2. For this chamber this factor is .321 m^2 -steradian^2.

Table V gives the flux measured by this experiment of the various heavy components of the cosmic ray beam.

SUMMARY OF THE BACKGROUND CORRECTION

In any critical analysis of the results of this experiment it is necessary to have well in mind any approximations made in correcting for the background counting rate. For this reason we now summarize the steps that were involved in the background correction.

The counting rate of a pulse ionization chamber biased so that only minimum ionizing particles of about $Z \geq 3$ are detected consists of the following:

(a) Cosmic ray primaries of $Z \geq 3$

(b) Fragments of heavy primary particles

(c) Nuclear star evaporation particles

(d) Slow secondary protons produced in the collisions of the primary and secondary flux with the atmosphere and the material surrounding the chamber

(e) Slow α-particles

(f) Electron shower particles

(g) Pileup of small pulses producing a detectable pulse.

In order to find the cosmic-ray flux at the top of the atmosphere, the counting rate of the chamber must be corrected for items (b)-(g). Item (b) was corrected for by solving the diffusion equations which includes the fragmentation particles.

The correction for extrapolating to the top of the atmosphere was large because of the chamber's apparent depth in the atmosphere of 32 g/cm^2. Equations 72a, 72b, and 72c show that this correction consisted essentially of having to multiply the sphere counting rate by factors between 2.7 and 4. Any errors in the parameters of the diffusion equations will be reflected more in this experiment than in those of most other observers, whose depth of observation has been between 10 and 25 g/cm^2.

The nuclear star evaporation particle correction was accomplished by a combination of calculation and experiment. Using the data from photographic emulsions on the production and the characteristics of nuclear stars, a calculation was made, with certain simplifying assumptions, to give a sufficiently accurate determination of the counting rate expected in the chamber due to nuclear stars, and some characteristics of the distribution in size of the pulses. In particular, it gave the ratio of the counting rate in Chamber No. 14 to the counting rate in Chamber No. 13 caused by nuclear stars. The experiment consisted of simultaneously sending up on a skyhook balloon two chambers identical in all respects except that one chamber, No. 14, had 2.14 times the argon pressure of the other chamber, No. 13. The pulse size distribution due to evaporation particles from nuclear stars stopping in the chamber will be independent of the pressure but will depend only on the energy distribution of

evaporation particles. The pulse sizes due to cosmic rays will be directly proportional to the pressure. By comparing the counting rates of Chambers No. 13 and No. 14 it is possible, using the results of the calculation, to determine an experimental integral pulse height distribution caused by the particles that stop in the chamber.

The pulses due to the evaporation star particles that pass through the chamber were not corrected for, but only that part of the data was used where it was shown that the number of these pulses should be small.

Slow secondary protons, mainly the "grey" proton product from nuclear stars, could produce detectable pulses. A calculation was performed which showed that for the part of the data used the contribution of these pulses should be small.

Slow α-particles capable of producing detectable pulses can be produced by a portion of the primary α-particles losing energy by ionization before reaching the chamber. This effect was calculated and was corrected for. Slow α-particles are also produced in nuclear stars and the fragmentation of the heavier cosmic-ray flux in the atmosphere. The slow α-particles in nuclear stars were already taken into account by the nuclear star corrections. Because the heavier flux is much smaller than the α-particle flux, the number of α-particles produced in the fragmentation of the heavier is also much smaller than the primary α's. In

addition, their energy distribution at the chamber will not be much different. The effect of these fragments was accounted for by increasing slightly the assumed primary α-particle flux.

It was shown that both electron showers and the pileup of small pulses produce only a negligible contribution to the counting rate.

DISCUSSION OF DATA

The results of other observers on the measurement of the heavy flux are shown in Table V. It is seen that the value of the heavy flux for this experiment agrees reasonably well with the other investigators' values. However, the values for the CNO group and the Be B group, as measured by this experiment, are higher than the other investigators' values. The values given by the other investigators are for the CNOF group. Since the evidence indicates that the abundance of fluorine is very small the values for CNO and CNOF should be very closely the same. As is noticed if one takes the lower limit of the values of this experiment there is a reasonable agreement with the Bristol data.[19]

This may indicate that the high values for the CNO group are caused by the uncertainties in the background correction. There was no indication that the equipment was misbehaving during the flight. The Po-α pulses showed that both the receiving and transmitting equipment were functioning properly. As a further check the counting rate of Chamber No. 13 agreed reasonably well with the counting rate as measured by Coor [9] under approximately the same conditions.

The background effects in items (c) and (d) that have not been corrected for because they were considered small enough to neglect, plus any others that have not been con-

sidered, will increase the measured flux values above their true ones. These effects should become of relatively less importance as the pulse size increases, and thus we might expect, if these effects are present, the L group measurement to be higher than the true value by the greatest amount. An estimate of this effect can be obtained by calculating the L flux from the following three sets of data:

I data in Figure 14 from 5.7 to 11.4 volts
II data in Figure 14 from 6.9 to 11.4 volts
III data in Figure 14 from 8.6 to 11.4 volts.

If the suspected effect is large and its importance decreases with pulse size relatively faster than cosmic rays do, then the measured flux values should decrease from Data Set I to Data Set III. From the calculated flux values given in Table VI it is seen that there may be such a tendency. To minimize this effect the result of Data Set III is used as the correct value of the Be B flux.

It is felt that there is really no significant difference between the CNO flux values of this experiment and the values of other observers. The uncertainty in the background correction can account for the difference. The background effects that have not been corrected for because they were considered small enough to neglect should not be of any importance in that part of the data used in determining the CNO flux. However, as is seen in Figure 18 there are large uncer-

Table VI. Be and B flux values calculated for different sets of data to determine the importance of the neglected background

Group Type	Be and B Primary Flux Values (particles/m^2-steradian-sec.)
I	32±12
II	30.2±12
III	22.5±13

tainties in $B^{14}(S)$. To determine $B^{14}(S)$ it was necessary to take a difference between two counting rates where the difference was, for the smaller values of S, about 10 to 20 percent of each rate. There was an uncertainty in the pulse size measurement of about 5 percent. At these smaller values of pulse size a 5 percent error in the pulse size produces a 10 percent error in the counting rate. This error in the pulse size determination and the statistical errors produce the large uncertainty in $B^{14}(S)$ shown in Figure 18. The large errors in the flux values were due almost entirely to the uncertainty in $B^{14}(S)$.

The measurement of perhaps greatest interest is the value obtained for the Be and B flux. It would be extremely difficult to account for the increase in the counting rate of Chamber No. 14 between 5.7 and 11.4 volts without assuming the presence of Be and B in the primary beam. Though the exact flux of Be and B, as determined by this experiment, is uncertain, it is felt that the presence of Be and B in the primary beam is unquestionable. This experiment agrees with the Bristol group [19] in showing that the primary flux of Be and B is about as plentiful as CNO.

It was not possible in this experiment to obtain any quantitative data on the abundance of Li in the primary cosmic-ray beam. At the pulse sizes where Li gives its greatest contribution, the counting rate included a large but indeterminable contribution from slow secondary protons.

This part of the data was consequently neglected. However, the portion of the data which was used in determining the flux of Be and B included about 9 percent of the Li flux. It was assumed that Li produced 4 counts per second in the chamber in order to give a small correction to the Be and B flux value.

Because of ionization losses not all of the heavy flux incident on the top of the atmosphere will affect the chambers. The range of particles with Z = 14 and ε (energy per nucleon) equal to the cutoff value of .3 Bev is only 8.6 g/cm^2 of air. The lowest energy per nucleon effective in producing counts in the chambers for the various charge groups is shown in Table V.

CONCLUSIONS

The data of this experiment indicate, with not as much accuracy as would be desired, that Be and B are present in the primary cosmic-ray beam with about the same abundance as the C N O group. The significance of this as regards the origin of the cosmic rays has been amply discussed by various investigators,[19,20,21] and it would be redundant to repeat their arguments. However, it should be pointed out that it is of importance to determine the relative abundance of Li, Be, and B among themselves. Except for Li, Be, and B, the abundances of the elements in the cosmic-ray beam approximate their abundances in our galaxy. In this picture, the relatively large abundances of Li, Be, and B compared to their abundances in the galaxy can be explained by saying that Li, Be, and B were not accelerated at the source like the other elements but are the fragments of the heavier particles. If this is the actual case, then emulsion data [18] indicate that Li should be as abundant as both Be and B combined. If it can be thus shown that primary Li, Be, and B are entirely fragmentation products from collisions in interstellar matter, then the lifetime of the heavy cosmic rays can be determined. However, until this is done, one cannot draw any conclusions about the lifetime of the heavy cosmic rays.

Nuclear stars produced about a constant fraction of one-third of the Chamber No. 14 counting rate for all pulses greater than .4 Po-α pulse through to all pulses greater than 2.7 Po-α pulse. The ionization due to these nuclear stars is 7 percent of the total ionization measured at approximately the same altitude, latitude, and time.[22] Although this percentage of the total ionization was measured with 3.17 atmospheres argon pressure, it is the same for all pressures since both the total ionization and the ionization due to stars vary approximately proportionally to the pressure.

It is feasible to account for the background pulses in a pulse ionization chamber and obtain values for the cosmic-ray flux. This experiment far from exhausts the ultimate accuracy possible. The amount of star background can be halved relative to the heavy cosmic rays by requiring a coincidence between a geiger counter and the chamber, since one-half of the stars are produced by neutrons. The star background can be relatively further reduced by using a vertical counter telescope in coincidence with the pulse chamber. This has the effect of decreasing the apparent depth of the chamber, and, consequently, the heavies will be less attenuated. The counting rate caused by slow protons can be eliminated and data obtained on the Li flux. One way to do this would be to place the ion chamber inside the counter telescope and place 4 g/cm^2 of aluminum absorber between the chamber and the lower counter. By requiring a

coincidence between the chamber and the telescope, protons less energetic than 60 Mev will be eliminated, since they will stop in the absorber before discharging the lower counter.

Unfortunately, all such refinements will increase the complexity and weight of the equipment. Since for balloon flights small weight and simplicity of equipment are of extreme importance, it is worthwhile to determine what can be done to improve the equipment of this experiment without appreciably complicating it. We will then attempt to determine what information can be obtained by the improved version.

One serious disadvantage of the equipment of this experiment is the long length of time required for collecting enough data. As was explained, this was due to the method used for measuring pulse sizes. One loses the advantage gained by small weight, which permits lifting of the equipment much more cheaply and conveniently with small balloons, by requiring long lengths of time at altitude to obtain the necessary statistics. Thus, although when batteried for a 4-hour flight the completely wrapped equipment weighed only $9\frac{1}{2}$ pounds, it was still necessary to lift the equipment on a large skyhook balloon in order to keep it at high altitude the required time.

It is not necessary anymore to obtain the fine detail in the integral pulse height distribution curve as was done

in this experiment (Figure 14). This experiment showed that once the star correction is known it is only necessary to know the counting rate at three voltages, namely 8.6 volts = .66 Po-α pulse, 11.4 volts = .88 Po-α pulse, and 28.6 volts = 2.2 Po-α pulse. The difference in the counting rate between 8.6 volts and 11.4 volts, corrected for the star contribution, gave the information on the Be and B flux. The difference between 11.4 volts and 28.6 volts, corrected for the star contribution, gave the information on the CNO flux. The counting rate at 28.6 volts, corrected for the star contribution and the counts caused by $Z \leq 8$, gave the information on the $Z \geq 9$ flux.

We could still have obtained the same information on the flux of the various heavy particle groups by choosing 12.2 volts = .94 Po-α pulse instead of 11.4 volts. At 12.2 volts there is the added advantage that at that voltage one can measure changes in the amplifier gain. From Figure 6 it is seen that at the constant voltage which passes initially all pulses greater than .94 Po-α pulse, the counting rate of the Po α-particles would decrease very fast with any decrease in the amplifier gain.

To determine the star correction this experiment has shown that it is necessary to determine the counting rate at only one other voltage for the full pressure chamber, namely at about 90 volts in Chamber No. 14 or as large a voltage as possible. If the lower pressure chamber (No. 13

in this experiment) is filled to 1/R the pressure of the full pressure chamber, then it is necessary to determine the counting rate in this chamber at the pulse sizes

$$\frac{V_i}{R} \; S_{Po-\alpha}^{max\ 13}, (i = 1,2,3,4)$$

where

$$V_1 = .66,\ V_2 = .94,\ V_3 = 2.2,\ S_{Po-\alpha}^{max\ 13}\ V_4 = 90 \text{ volts}$$

or the maximum possible voltage, and $S_{Po-\alpha}^{max\ 13}$ and $S_{Po-\alpha}^{max\ 14}$ are the maximum pulses due to Po α-particles in the lower and higher pressure chambers respectively (the Po-α pulse voltages).

It should be cautioned that the full pressure and lower pressure chambers should have their various voltages very accurately determined because B(S) is very sensitive to these voltages. In this experiment uncertainties in the values of the pulse voltages of less than 5 percent produced the large uncertainties in the background correction $B^{14}(S)$ (Figure 18).

By this means of measuring the counting rate at only four different voltages, it would be necessary to gather the data at the maximum altitude for only 15.6 minutes to obtain greater statistical accuracy than was obtained from the 4 hours of good data of this experiment. Because the information is obtained by taking the difference between the counting

rates at the three smallest voltages (V_1, V_2, V_3), the best statistical value of this difference is obtained when the time of measurement at these voltages is proportional to the square root of the rates at these voltages. The time spent at the highest voltage, V_4, is determined to give a statistical accuracy of about 10 percent. These requirements are fulfilled when the times spent at V_1, V_2, V_3, and V_4 are 3.2 minutes, 1.4 minutes, 1.0 minute, and 10 minutes, respectively.

Periodically the Po α-particles should be turned on to calibrate the amplifier gain. With this modified arrangement it is possible to obtain with much smaller balloons a more accurate measurement of the heavy primary flux. The statistics would be better, and the voltages could be measured more accurately since they can be taken off of a bias battery.

Once the contribution of the star background is determined it will not be necessary to take any more measurements at V_4, and all the necessary data can be obtained in 5.6 minutes at altitude.

The optimum pressures to use in the chambers appear to be the ones used in this experiment. Higher pressures would require a greater voltage across the ion chamber electrodes to collect all of the electrons. Lower pressures would increase the star background relative to the cosmic-ray flux at a given pulse size.

The above discussion was specifically for flights made at about $\lambda = 55^{\circ}$. However, the same simplified equipment can be used at lower latitudes without any modification. It is possible to use the equipment for measuring the heavy primary flux at higher latitudes, but then one would have to know the energy spectrum of the primaries more accurately to calculate the theoretical integral pulse height distribution expected in the chamber due to the non-relativistic particles. However, the result should not be too sensitive to the assumed energy spectrum since the very low energy particles will not be able to reach the chamber because of their small ranges.

The interpretation of the data at all latitudes should be very similar. The calculations performed in this paper on the star background will hold for all latitudes, but it should be noted that they were made only for the argon pressures of this experiment. B(S) can be determined for all latitudes in the same way as was done in this experiment. In determining the flux, the theoretical integral pulse height distributions of cosmic-ray particles will vary from high latitudes to the lower latitudes because of non-relativistic particles, but once this is accounted for, the procedure is analogous for all latitudes.

There is a possibility that this simplified version of the pulse ionization chamber may be able to measure changes in the heavy flux of 10 percent or less. The limiting factor in this respect is uncertainties in the star background

correction. This correction is based on calculations of the relative star effects in the two different pressure chambers. The approximations made in this calculation may cause errors in the star background correction as large as 25 percent. If there is a fluctuation in the star-producing flux, this will cause a change in the counting rate of the chambers even though the heavy flux may stay constant. If the star correction is exact it will reflect this change and will give the correct value for the heavy flux. If the star correction is incorrect by 25 percent, and the star producing flux changes by 20 percent, there will be an apparent change in the heavy flux of only about 2 percent. It should be kept in mind that the star correction is only about one-third of the total counting rate and that the remaining two-thirds is due to the heavy nuclei.

The simplest version of the pulse ionization chamber using only the three voltages V_1, V_2, and V_3 and no correction made for the star background can still give information on the fluctuations of the heavy primaries. Let us say that the total intensity changed by 20 percent. If the counting rate in the pulse ionization chamber also changed by the same amount, then one could conclude that the intensity of the heavies also changed by 20 percent. If the heavy flux had remained constant there would be only a 6.7 percent change in the chamber counting rate.

It is felt that perhaps the most important use of this

simplified pulse ion chamber will be in measuring changes with time in the heavy particle flux and relative changes among the various heavy nucleus groups. In particular, changes during a solar flare or during the solar cycle can be readily measured by this instrument.

With the slight modification of also measuring the counting rate at V_4 and making measurements once at a given latitude with the lower pressure chamber, it should be possible to obtain a measure of the primary flux of the various heavy-particle groups. By this means it should be possible to obtain the latitude effect of the heavy particles and thus their energy spectrum. However, for greater accuracy it seems desirable to decrease the background by adding the counter telescope as described previously.

It is known that the total cosmic-ray intensity increases spectacularly during certain large solar flares, perhaps as much as 500 percent. There is evidence that even small flares produce smaller increases. This increase is believed to be due to particles coming directly from the sun. It is not known yet if the heavy particle intensity also increases during these flares. It would be of extreme interest to determine if this is so, since it would mean that these heavy particles come directly from the sun.

REFERENCES

1. Pomerantz and McClure, Phys. Rev. 86, 536 (1952)
2. Rossi and Staub, Ionization Chambers and Counters (McGraw-Hill Book Co., Inc., 1949), Chap. 3
3. G. W. McClure, Phys. Rev. 87, 680 (1952)
4. B. Rossi, High Energy Particles (Prentice-Hall, Inc., New York, 1952), p. 47
5. H. S. Bridge, W. E. Hazen, B. Rossi, and R. W. Williams, Phys. Rev. 74, 1083 (1948)
6. L. D. Landau, J. Phys. U.S.S.R. 8, 201 (1944)
7. Reference 4, p. 32-35
8. Reference 6, Equation 5
9. T. Coor, Jr., Phys. Rev. 82, 478 (1951)
10. Briggs, Rev. of Mod. Phys. 26, 1 (1954)
11. Camerini, Lock and Perkins, Progress in Cosmic Ray Physics Vol. I (North Holland Publishing Co., Amsterdam, 1952). The information on nuclear stars in this section was obtained from this reference, unless stated otherwise.
12. J. J. Lord, Phys. Rev. 81, 901 (1951)
13. Reference 4, p. 489
14. Kraybill, Phys. Rev. 76, 1092 (1949)
15. See, e.g., S. O. Rice, Bell System Tech. J. 23, 282 (1944)
16. Kaplon, Peters, Reynolds, and Ritson, Phys. Rev. 85, 295 (1952)

17. Noon and Kaplon, Phys. Rev. 97, 769 (1955)

18. Kaplon, Noon, and Racette, Phys. Rev. 96, 1408 (1954)

19. Dainton, Fowler, and Kent, Phil. Mag. 43, 729 (1952)

20. Bradt and Peters, Phys. Rev. 80, 943 (1950)

21. Peters, B. reference 11.

22. H. V. Neher (Private communication)

23. G. W. McClure, Phys. Rev. 96, 1391 (1954)

24. Forbush, J. of Geophy. Research 59, No. 4, 525 (1954)